Suppression of Heterotopic Ossification in Fibrodysplasia Ossificans Progressiva Using AAV Gene Delivery

Yeon-Suk Yang
University of Massachusetts Medical School
Jung-Min Kim
UMASS MEDICAL SCHOOL https://orcid.org/0000-0002-9072-4293
Jun Xie
University of Massachusetts Medical School https://orcid.org/0000-0001-9565-1567
Sachin Chaugule
University of Massachusetts Medical School
Chujiao Lin
University of Massachusetts-Medical School
Hong Ma
University of Massachusetts Chan Medical School
Edward Hsiao
UCSF https://orcid.org/0000-0001-8924-106X
Jaehyoung Hong
Korea Advanced Institute of Science and Technology
Hyunho Chun
Korea Advanced Institute of Science and Technology
Eileen Shore
University of Pennsylvania
Frederick Kaplan
University of Pennsylvania
Guangping Gao
University of Massachusetts Medical School https://orcid.org/0000-0003-0097-9012
Jae-Hyuck Shim (jaehyuck.shim@umassmed.edu)
University of Massachusetts-Medical School https://orcid.org/0000-0002-4947-3293

Article

Keywords:

Posted Date: June 10th, 2022

DOI: https://doi.org/10.21203/rs.3.rs-1646941/v1

Version of Record: A version of this preprint was published at Nature Communications on October 19th, 2022. See the published version at https://doi.org/10.1038/s41467-022-33956-9.

Suppression of Heterotopic Ossification in Fibrodysplasia Ossificans Progressiva Using AAV Gene Delivery

Yeon-Suk Yang[1+], Jung-Min Kim[1+], Jun Xie[3,4,5+], Sachin Chaugule[1], Chujiao Lin[1], Hong Ma[3,4,5], Edward Hsiao[6], Jaehyoung Hong[7], Hyonho Chun[7], Eileen M. Shore[8,9,11], Frederick S. Kaplan[8,10,11], Guangping Gao[2,3,4,5*], and Jae-Hyuck Shim[1,2,3*]

[1]Department of Medicine/Division of Rheumatology, University of Massachusetts Chan Medical School, Worcester, MA, USA

[2]Li Weibo Institute for Rare Diseases Research, University of Massachusetts Chan Medical School, Worcester, MA, USA

[3]Horae Gene Therapy Center, [4]Department of Microbiology and Physiological Systems, [5]Viral Vector Core, University of Massachusetts Chan Medical School, Worcester, MA, USA

[6]Division of Endocrinology and Metabolism, Department of Medicine; the Institute for Human Genetics; the Program in Craniofacial Biology; and the eli and Edyth Broad Institute of Regeneration Medicine, University of California-San Francisco, San Francisco, CA, USA

[7]Department of Mathematical Sciences, Korea Advanced Institute of Science and Technology, Daejeon, Republic of Korea

[8]Department of Orthopaedic Surgery, [9]Department of Genetics, [10]Department of Medicine, and [11]The Center for Research in FOP and Related Disorders, The Perelman School of Medicine at the University of Pennsylvania, Philadelphia, PA, USA

[+]These authors contributed equally to this work.

*To whom correspondence should be addressed:

Jae-Hyuck Shim

Department of Medicine/Division of Rheumatology, Horae Gene Therapy Center, Li Weibo Institute for Rare Diseases Research

University of Massachusetts Chan Medical School,

364 Plantation Street, LRB 217, Worcester, MA 01605

Tel.: 508-856-6245

Email: jaehyuck.shim@umassmed.edu

and

Guangping Gao

Horae Gene Therapy Center, Li Weibo Institute for Rare Diseases Research

University of Massachusetts Chan Medical School,

368 Plantation Street, AS6-2049, Worcester, MA 01605

Email: guangping.gao@umassmed.edu

Abstract

Progressive heterotopic ossification (HO) is the most disabling and defining feature of fibrodysplasia ossificans progressiva (FOP), an ultra-rare genetic disorder. More than 95% of FOP patients harbor a heterozygous activating mutation (c.617G>A;p.R206H) in the Activin A Receptor Type 1 (ACVR1). Currently, there are no definitive preventions or treatments. Gene therapy is thus an attractive treatment strategy. Here, we identify recombinant adeno-associated virus 9 (rAAV9) as the most effective serotype for transduction of the major cells-of-origin of HO in soft tissues. Using AAV-mediated gene delivery, three gene therapy approaches for FOP, including gene replacement by expression of codon-optimized human *ACVR1* (*ACVR1*^{OPT}), *ACVR1*^{R206H} allele-specific silencing by AAV-compatible artificial miRNA (amiR, amiR-*ACVR1*^{R206H}), and a combination of gene replacement and silencing (*ACVR1*^{OPT};amiR-*ACVR1*^{R206H}), were developed. AAV gene therapy ablated aberrant Activin A signaling and chondrogenic and osteogenic differentiation of mouse skeletal cells harboring a conditional knock-in allele of human *ACVR1*^{R206H} (*Acvr1*$^{(R206H)KI}$) and human FOP patient-derived induced pluripotent stem cells (iPSCs). Accordingly, trauma-induced HO was markedly reduced in *Acvr1*$^{(R206H)KI}$ mice treated locally in early adulthood or systemically at birth. These mice displayed a significant decrease in endochondral bone formation in injured muscle while inflammation and fibroproliferation responses to injury remained largely intact. Remarkably, spontaneous HO in juvenile and adult *Acvr1*$^{(R206H)KI}$ mice was also substantially decreased by AAV gene therapy. Compared to gene replacement or silencing, combination gene therapy was the most potent in preventing both traumatic and spontaneous HO in FOP mice. Collectively, our results identify novel gene therapeutics that can prevent disabling HO in FOP mice and provide evidence to support clinical translation to FOP patients.

Introduction

Fibrodysplasia ossificans progressiva (FOP, OMIM 135100) is an ultra-rare genetic disorder with a defining feature of progressive, disabling heterotopic ossification (HO) that forms within skeletal muscle, tendons, ligaments, fascia and aponeuroses[1,2]. HO develops in childhood and early adulthood during episodic flare-ups that occur spontaneously or are triggered by minor trauma, injury, intramuscular injection or inflammation[2]. The new bone leads to progressive immobility and severe pain[2].

All patients with FOP have gain-of-function mutations in the bone morphogenetic protein (BMP) type I receptor *ACVR1*, and ~97% of FOP patients harbor a recurrent *ACVR1*^{R206H} mutation (c.617G>A;p.R206H)[3,4]. Recent studies showed that *ACVR1*^{R206H} confers dysregulated BMP-pSMAD1/5 signaling in response to Activin A, which normally inhibits BMP signaling through the wild-type (WT) ACVR1 receptor[5,6]. Notably, the therapeutic effect of anti-Activin A antibody is specific to FOP, with no effect on acquired forms of HO, suggesting that Activin A acts as a congenic ligand of the *ACVR1*^{R206H} receptor[7,8]. Although multiple cell types leading to HO, such as Tie2^{+} endothelial cells[9], Scx1^{+} cells[10], and PDGFRα^{+}Sca1^{+} fibroadipogenic progenitors (FAPs)[11], have been identified[12], FAPs appear to be the most consistent cell type and major contributor to HO. However, molecular mechanisms of such findings in coordination with a niche environment have yet to be fully elucidated.

FOP treatment is challenging due to the early age of onset of ectopic bone formation and the difficulty in selectively suppressing BMP signaling by the *ACVR1*^{R206H} mutation. Presently, there is no definitive prevention or treatment for the progressively disabling HO except for symptomatic management with high-dose corticosteroids for episodic flare-ups, which can reduce symptoms like pain and edema[13]. Although several new drugs, including a retinoic acid receptor γ agonist (palovarotene), an anti-Activin A antibody (REGN 2477), an immunosuppressant (rapamycin), and ACVR1 kinase inhibitors (IPN60130), are currently in clinical trials, use of these drugs is limited[14]. Given that gene therapy using recombinant adeno-associated viral (rAAV) vectors holds promise for treating many genetic disorders[15], AAV gene therapy may be a plausible therapeutic strategy for FOP. rAAVs have demonstrated high transduction efficiencies to skeletal muscle and the skeleton *in vivo*,[16,17]

long-term durability of therapeutic gene expression[18], and acceptable safety profiles in clinical studies. Of note, rAAVs have been evaluated in over 145 clinical trials and 2,000 patients worldwide[19].

This study identifies AAV gene therapy as a promising therapeutic option for blocking HO in FOP. We demonstrate that the rAAV9 serotype effectively transduces the identified cells-of-origin of HO, FAPs in mice harboring a conditional knock-in allele of human *ACVR1*^{R206H} (*Acvr1*$^{(R206H)KI}$). *Acvr1*$^{(R206H)KI}$ mice can be used to test the efficacy of AAV gene therapy on the skeletal and extraskeletal features of FOP as they model both the skeletal malformations and progressive HO found in human FOP patients[7]. Remarkably, AAV-mediated delivery of gene replacement, *ACVR1*^{R206H} allele-specific silencing, or a combination of gene replacement and silencing, was highly effective in suppressing both traumatic and spontaneous HO in these mice when administered t.d. or i.v. at birth or early adulthood. Mechanistically, AAV gene therapy ablated aberrant Activin A signaling and chondrogenic and osteogenic differentiation of human FOP patient-derived iPSCs and mouse *Acvr1*$^{(R206H)KI}$ skeletal cells. Taken together, our proof-of-concept study using AAV gene therapy provides fundamental insights into a critical step toward clinical translation for FOP patients.

Results

AAV gene therapy targets the human *ACVR1*^{R206H} receptor

FOP is caused by a heterozygous, activating mutation of *ACVR1* (c.617G>A;p.R206H) in approximately 97% of patients[4]. Given recent evidence that wild-type ACVR1 (*ACVR1*^{WT}) blocks BMP signaling and leads to an inhibition of HO in FOP mice[11], we hypothesized that dilution of dysregulated BMP signaling of *ACVR1*^{R206H} with overexpressed *ACVR1*^{WT} might inhibit dysregulated BMP signaling and HO in FOP (hereafter, referred to gene replacement, **Extended Data Fig. 1**). To inhibit the dysregulated BMP signaling of human *ACVR1*^{R206H}, a codon-optimized version of human *ACVR1* complementary DNA (*ACVR1*^{opt}, 74% nucleotide identity compared to wild-type coding sequence) was cloned into the AAV vector genome containing a CMV enhancer, chicken β-actin promoter (CBA), and intron. To reduce the size of the AAV vector, the 1027 bp CBA intron was replaced by a 384 bp MassBiologics (MBL) intron or a 172 bp synthetic intron (**Fig. 1a**), validating abundant expression of the *ACVR1*^{opt} receptor driven by all three promoters (**Fig. 1b**). Since high levels of AAV-delivered shRNAs can perturb native RNAi machinery and cause off-target silencing effects[20,21], we developed AAV-compatible artificial miRNA (amiR) by inserting the guide strand of a small silencing RNA into a mouse miR-33-derived miRNA scaffold, which substantially improved conventional shRNA-related toxicity and off-target silencing[22]. Using a sequence walk methodology, twelve amiRs targeting human *ACVR1*^{R206H} mRNA, but not human *ACVR1*^{WT} and *ACVR1*^{opt} mRNAs, were designed and inserted in the intron between the CBA promoter and the mCherry reporter gene (**Fig. 1c**). Additionally, the sensor plasmids encoding firefly luciferase (Fluc), *Renilla* luciferase (RLuc), and complimentary sequences of human *ACVR1*^{R206H}, *ACVR1*^{WT}, or *ACVR1*^{opt} in 3'-UTR of RLuc, were generated to screen *ACVR1*^{R206H} allele-specific *amiRs* (**Extended Data Fig. 2a**). RLuc activity was normalized to Fluc activity and lower luciferase activity represents higher silencing efficiency of amiRs (**Fig. 1d**). Moreover, mammalian expression vectors of human *ACVR1*^{R206H}, *ACVR1*^{WT}, or *ACVR1*^{opt} were co-transfected with amiRs, and protein or mRNA levels of ACVR1 receptor were assessed (**Fig. 1e, Extended Data Fig. 2, b and c**).

Among the twelve amiRs, *amiR-RH6* and *amiR-RH7* were selected as the most effective gene silencers specific to *ACVR1*^{R206H}, with little to no silencing effect on *ACVR1*^{WT} and *ACVR1*^{opt}. Finally, the combination of *amiR-RH6* or *amiR-RH7* and *ACVR1*^{opt} cDNA was cloned into the AAV vector genome containing the CBA promoter with MBL or synthetic (Syn) intron (**Fig. 1f**). The knockdown efficiency of *ACVR1*^{R206H} receptor by *amiR-RH6* or *amiR-RH7* (**Fig. 1g**), protein levels of *ACVR1*^{opt} receptor (**Fig. 1h**), and the ability of these plasmids to inhibit Activin A-induced luciferase activity (**Fig. 1i**). Thus, AAV plasmids designed to reduce the dysregulated signaling by *ACVR1*^{R206H} through gene replacement with *ACVR1*^{opt} expression, through gene silencing by *ACVR1*^{R206H} allele-specific amiRs*,* or through the combination (**Extended Data Fig. 1**) were successfully generated and their functions were validated *in vitro*.

AAV gene therapy inhibits osteogenic potentials of human FOP iPSCs

To identify the optimal AAV serotype for transducing human and mouse osteogenic progenitors *in vitro*, a self-complementary AAV (scAAV) vector genome expressing the enhanced green fluorescent protein (*Egfp*) reporter gene was packaged into 15 conventional AAV capsids (rAAV1, rAAV2, rAAV2-TM[23], rAAV3b, rAAV4, rAAV5, rAAV6, rAAV6.2[24], rAAV7, rAAV8, rAAV9, rAAVrh8, rAAVrh10, rAAVrh39, and rAAVrh43)[25], and incubated with induced pluripotent stem cells (iPSCs) derived from dermal fibroblasts of human FOP patients[26,27], human bone marrow-derived mesenchymal stromal cells (BMSCs), human adipose-derived mesenchymal stromal cells (ASCs)[28,29], or mouse skeletal muscle progenitors (C2C12). Expression of EGFP in transduced cells was assessed by immunoblotting (**Fig. 2a**) and fluorescence microscopy (**Extended Data Fig. 3**). Four AAV serotypes, rAAV2, rAAV5, rAAV6, and rAAV6.2, were able to transduce all four cell types, while rAAV4 was only able to transduce ASCs and C2C12 cells, and rAAV9 was only able to transduce BMSCs. Since rAAV6.2 showed the highest transduction efficacy in all four cell types, the constructs expressing *amiR-RH6* or *amiR-RH7* and *ACVR1*^{opt} were packaged into the AAV6.2 capsid, and their genome integrity was validated (**Fig. 2b**).

Since large amounts of tissue from FOP patients cannot be obtained due to the substantial risks of inducing more HO, human FOP iPSCs were generated. iPSCs have been well established for *in vitro* FOP modeling and for applications in drug screening[26,27,30]. To test effects of AAV gene therapy on human FOP iPSCs *in vitro*, cells were transduced with rAAV6.2 carrying *egfp* (control), *amiR-RH6.ACVR1^{opt}* or *amiR-RH7.ACVR1^{opt}* (combination therapy). Silencing specificity of *amiR-RH6 or -RH7* was examined by next-generation sequencing (NGS), demonstrating that while EGFP control-expressing FOP iPSCs displayed 65.4% *ACVR1^{R206H}* vs. 34.6% *ACVR1^{WT}* transcripts, the transcript pattern was substantially shifted to 36.7% vs. 63.3% (*amiR-RH6.ACVR1^{opt}*) and 39.5% vs. 60.5% (*amiR-RH7.ACVR1^{opt}*, **Fig. 2c, top**). Expression of *ACVR1^{opt}* and EGFP was also confirmed in these cells (**Fig. 2c, bottom, Extended Data Fig. 4a**). Whole transcriptome analysis further demonstrated that compared to control, *amiR-RH6.ACVR1^{opt}* and *amiR-RH7.ACVR1^{opt}* induced upregulation of 45 and 140 genes and downregulation of 27 and 87 genes, respectively (**Fig. 2d**), whereas the numbers of differentially expressed genes were markedly reduced to 8 (upregulation) and 1 (downregulation) genes when comparing *amiR-RH6.ACVR1^{opt}* and *amiR-RH7.ACVR1^{opt}* (**Extended Data Fig. 4b**). These results suggest similar silencing specificity of *amiR-RH6* and *amiR-RH7*. Finally, we examined the ability of these AAVs to suppress osteogenic differentiation of FOP iPSCs and demonstrated a significant decrease in alkaline phosphatase (ALP) activity (an early osteogenic marker), mineral deposition (a late osteogenic marker), and mRNA expression of *RUNX2* (a marker of early osteoblastic gene expression, **Fig. 2e and f**). Since only *amiR-RH6.ACVR1^{opt}* treatment did not alter ALP, mineralization, or *RUNX2* expression in human WT iPSCs generated from healthy donors, the therapeutic effects of *amiR-RH6.ACVR1^{opt}* might be more specific to the human *ACVR1^{R206H}* mutation in iPSCs than those of *amiR-RH7.ACVR1^{opt}*.

Previous studies demonstrated that the *ACVR1^{R206H}* mutation activates SMAD1/5-mediated BMP signaling in response to Activin A, whereas Activin A does not normally activate BMP-pSMAD1/5 signaling via the ACVR1^{WT} receptor[6,5,7]. As expected, Activin A treatment significantly upregulated the expression of BMP-responsive genes, *ID1* and *MSX2*, in control-expressing FOP iPSCs, but this

induction was markedly reduced in the presence of *amiR-RH6.ACVR1^{opt}* or *amiR-RH7.ACVR1^{opt}* (**Fig. 2g, Extended Data Fig. 4c**). Thus, the combined approach of silencing *ACVR1^{R206H}* expression and expressing the ACVR1^{opt} receptor is a potent inhibitor of Activin A-induced aberrant BMP signaling and osteogenic differentiation in human FOP iPSCs.

AAV gene therapy suppresses dysregulated BMP signaling in mouse *Acvr1$^{(R206H)KI}$* skeletal cells

Given that FAPs were identified as the cell-of-origin of HO in a mouse model of FOP[11,12], a subset of FAPs were isolated from the skeletal muscle of 4-week-old *Acvr1$^{(R206H)Fl}$;PDGFR*α-cre mice using cell surface markers (PDGFRα^{+}ScaI^{+}CD31^{-}CD45^{-})[11]. As seen in human FOP iPSCs, treatment with *amiR-RH6.ACVR1^{opt}* or *amiR-RH7.ACVR1^{opt}* resulted in a significant decrease in Activin A-induced ALP activity and osteogenic gene expression (**Fig. 2h and i**). These results demonstrate therapeutic effectiveness of combination treatment in both human and mouse FOP cells.

To further define the potential therapeutic effects of *ACVR1^{R206H}* allele-specific silencing, gene replacement, or the combination in FOP, rAAV6.2 carrying *amiR-RH6*, *ACVR1^{opt}*, or *amiR-RH6.ACVR1^{opt}* were transduced into mouse *Acvr1$^{(R206H)KI}$* osteogenic progenitors isolated from *Acvr1$^{(R206H)Fl}$;PRRX1-cre* mice. Knockdown efficiency of *ACVR1^{R206H}* and expression of *ACVR1^{opt}* were validated in these cells (**Extended Data Fig. 5a**). Since *amiR-RH6.ACVR1^{opt}* shows a higher specificity to the human *ACVR1^{R206H}* mutation in iPSCs than *amiR-RH7.ACVR1^{opt}* (**Fig. 2d-f**), *amiR-RH6.ACVR1^{opt}* and *amiR-RH6* were selected for further studies. *amiR-RH6.ACVR1^{opt}* markedly reduced Activin A-induced SMAD1/5 phosphorylation and *Id1* expression in *Acvr1$^{(R206H)KI}$* cells, whereas little to mild reduction was detected in the presence of *amiR-RH6* or *ACVR1^{opt}* alone, compared to EGFP control (**Fig. 3a and b**). Notably, control-expressing *Acvr1$^{(R206H)Fl}$* (*Acvr1^{WT}*) cells were unresponsive to Activin A. As a result, ALP and mineralization activities of *Acvr1$^{(R206H)KI}$* osteogenic progenitors were more reduced by *amiR-RH6.ACVR1^{opt}* than *amiR-RH6* and *ACVR1^{opt}*, demonstrating inhibitory effects of this combination strategy on both early and late osteogenic differentiation (**Fig. 3c, Extended Data Fig. 5b-**

d). This inhibitory effect is specific to Activin A-induced osteogenesis of *Acvr1*$^{(R206H)KI}$ cells since BMP4-induced mineralization in these cells was not affected by *amiR-RH6.ACVR1*^{opt} (**Fig. 3d**).

Next, we tested therapeutic effects of AAV gene therapy on Activin A-induced chondrogenesis of *Acvr1*$^{(R206H)KI}$ chondrogenic progenitors isolated from the knee joints of *Acvr1*$^{(R206H)Fl}$*;PRRX1-cre* neonates at postnatal day 2 (P2). After AAV treatment, knockdown efficiency of *ACVR1*^{R206H} and expression of *ACVR1*^{opt} were validated in these cells (**Extended Data Fig. 5e**). *amiR-RH6.ACVR1*^{opt} almost completely ablated Activin A-induced chondrogenesis, as shown by significant decrease in the expression of early (Sox9 and Type 2 Collagen) and late (Aggrecan) chondrogenic genes and the production of cartilage matrix proteoglycans (alcian blue staining) (**Fig. 3e, Extended Data Fig. 5f**). Collectively, these results suggest that AAV-mediated delivery of a combined *ACVR1*^{R206H} allele-specific amiR and *ACVR1*^{opt} could potently suppress Activin A-induced aberrant BMP signaling, osteogenesis, and chondrogenesis of human and mouse FOP cells, with little to no effect on the ACVR1^{WT} receptor-mediated signaling and BMP-induced signaling.

Local delivery of AAV gene therapy suppresses traumatic HO in *Acvr1*$^{(R206H)KI}$ FOP mice

Determining the transduction efficiencies of rAAVs *in vitro* is essential to test different AAV-based strategies in relevant cell types; however, the efficacy of an rAAV *in vivo* is impacted by multiple factors, including the route of administration, serum factors, circulating neutralizing antibodies, and multiple physiological barriers including the ability to evade immune activation[25]. Therefore, to examine the ability of rAAV6.2 to transduce the skeletal muscle where HO primarily develops in FOP mice, rAAV6.2.*egfp* was administered intravenously (i.v.) to mice, and EGFP expression in individual tissues was monitored by IVIS-100 optical imaging (**Extended Data Fig. 6a**). As previously reported[31], EGFP expression was only detected in the liver, whereas the skeletal muscle (hindlimb) and heart showed weak expression when i.v. administered together with vascular agents, including recombinant vascular endothelial growth factor (VEGF)-166, sodium heparin, and serum albumin (**Extended Data Fig. 6b**).

Thus, rAAV6.2 was excluded as a candidate serotype for *in vivo* FOP gene therapy due its low transduction efficiency in the skeletal muscle.

For our *in vivo* experiments, we turned to rAAV9, as this serotype has been reported to be highly effective for transducing skeletal muscle and bone[16,17] and it can transduce ~80% of muscle-resident mesenchymal stem cells via intramuscular (i.m.) injection[32]. Our optical imaging data also confirmed a high transduction efficiency of i.v. administered rAAV9 in the skeletal muscle (**Extended Data Fig. 6c**). Since i.m. injection often induces muscle trauma in FOP patients, causing HO lesions[33], skeletal muscle was transduced with rAAV9.*mCherry* via transdermal (t.d.) injection using a hollow microneedle[34] to minimize muscle trauma (**Extended Data Fig. 6d and e**). To examine its ability to transduce HO-inducing FAP-lineage cells in the skeletal muscle via t.d. injection, a mouse model representing the highest incidence forms of HO, muscle trauma/BMP-induced HO[35,36], was employed in *Tie2-cre;Rosa26*^{mCherry} reporter mice that express mCherry in a subset of FAP-lineage cells and endothelial cells[9,37]. One week after blunted muscle injury and i.m. administration of recombinant BMPs and matrigel into the quadricep of 2-month-old mice, rAAV9.*egfp* was injected t.d., and three weeks later, HO and EGFP expression were assessed by radiography and fluorescence microscopy, respectively (**Extended Data Fig. 7a**). In addition to the muscle fibers, a subset of Tie2^{+} FAP-lineage cells and osteoblasts within forming HO lesions also showed EGFP expression (**Fig. 3f**) while little to no expression was detected in the HO lesions treated with rAAV6.2.*egfp* (**Extended Data Fig. 7b**). These results demonstrated that t.d. delivery of rAAV9, not rAAV6.2, can transduce skeletal muscle cells and Tie2^{+} FAP- and osteoblast-lineage cells within forming HO lesions.

Since constitutive expression of human *Acvr1*^{R206H} allele results in perinatal lethality in mice[38,39], mice harboring a conditional *Acvr1*^{R206H} knock-in allele (*Acvr1*$^{(R206H)Fl}$) were crossed with Cre-ER^{T2} mice (*Acvr1*$^{(R206H)Fl}$;Cre-ER^{T2}) where tamoxifen-induced expression of Cre recombinase mediates *Acvr1*^{R206H}-driven HO in early adulthood. Traumatic HO was induced by tibial muscle injury in these mice four weeks after t.d. injection of rAAV9 expressing the Cre recombinase (**Extended Data Fig. 7c**). Cre-mediated expression of *Acvr1*$^{(R206H)KI}$ in the gastrocnemius muscle resulted in HO following pinch

injury/cardiotoxin injection (**Fig. 3g and h**), confirming the effectiveness of t.d. delivery of rAAV9 to HO-inducing cells in skeletal muscle.

To examine the ability of AAV gene therapy to suppress trauma-induced HO in FOP mice, 6-week-old *Acvr1*$^{(R206H)FI}$;Cre-ER^{T2} mice were treated with tamoxifen to induce Cre recombinase expression, followed by t.d. injection of rAAV9 carrying EGFP control, *amiR-RH6*, *ACVR1*^{opt}, or *amiR-RH6.ACVR1*^{opt}. Three days later, pinch injury/cardiotoxin injection was introduced into the gastrocnemius muscle (**Extended Data Fig. 7d**). Knockdown efficiency of *ACVR1*^{R206H} or *ACVR1*^{opt} expression in AAV-treated gastrocnemius muscle was validated four weeks after muscle injury (**Extended Data Fig. 7e**). AAV treatment significantly reduced HO in the gastrocnemius muscle (**Fig. 3i**), demonstrating that local delivery of *ACVR1*^{R206H} allele-specific silencing by *amiR-RH6*, gene replacement by *ACVR1*^{opt} expression, and the combination of both was all effective in suppressing trauma-induced HO in the skeletal muscle of FOP mice. Notably, as BMP4-induced osteogenesis of *Acvr1*$^{(R206H)KI}$ osteogenic progenitors treated with *amiR-RH6.ACVR1*^{opt} was largely intact (**Fig. 3d**), t.d. delivery of *amiR-RH6.ACVR1*^{opt} did not affect muscle trauma/BMP-induced HO (**Fig. 3j**), suggesting that therapeutic effectiveness of rAAV9.*amiR-RH6.ACVR1*^{opt} is specific to *ACVR1*^{R206H}-mediated genetic HO. Thus, AAV gene therapy is likely to act by inhibiting ACVR1^{R206H}-induced aberrant BMP signaling and resultant chondrogenesis and osteogenesis in the skeletal muscle of *Acvr1*$^{(R206H)KI}$ mice.

Systemic delivery of AAV gene therapy at birth prevents traumatic HO in *Acvr1*$^{(R206H)KI}$ FOP mice

All FOP patients with the classic *ACVR1*^{R206H} mutation present with great toe malformations at birth and experience episodic flare-ups following minor trauma and HO in childhood or early adulthood[13]. We examined the ability of AAV gene therapy given at birth to prevent trauma-induced HO in adult FOP mice. To examine whether systemic delivery of rAAV9 at birth can transduce HO-inducing FAP-lineage cells in the skeletal muscle, a single dose of rAAV9.*mCherry* was injected i.v. into P1 PDGFRα-GFP reporter neonates[40] (**Extended Data Fig. 8a**), demonstrating mCherry expression in a subset of

PDGFRα-GFP$^+$ FAP-lineage cells in the skeletal muscle and PDGFRα-GFP$^+$ osteoblasts and osteocytes in the trabecular and cortical bone compartments in addition to the heart, lung, liver, and kidney (**Fig. 4a, Extended Data Fig. 8b and c**). These results were also confirmed in WT mice treated with rAAV9 expressing β-galactosidase (rAAV9.LacZ, **Extended Data Fig. 8d**). Notably, no expression of GFP and mCherry proteins in the growth plate suggests that chondrocyte-lineage cells in the growth plate are negative for PDGFRα expression and not rAAV9-transducible. Thus, systemic delivery of rAAV9 at birth can transduce FAP-lineage cells in the skeletal muscle as well as osteoblast-lineage cells in the bone.

Next, rAAV9 carrying EGFP control, *amiR-RH6*, *ACVR1^{opt}*, or *amiR-RH6.ACVR1^{opt}* were administered i.v.to P1 *ACVR1$^{(R206H)Fl}$*;Cre-ER^{T2} neonates, and six weeks later, pinch injury/cardiotoxin injection was introduced to the gastrocnemius muscle three days after tamoxifen treatment (**Extended Data Fig. 8e**). Four weeks later, knockdown efficiency of *ACVR1^{R206H}* and *ACVR1^{opt}* expression in the gastrocnemius muscle was validated by RT-PCR analysis (**Fig. 4b**). Remarkably, *amiR-RH6.ACVR1^{opt}* ablated the development of heterotopic bone and chondrogenic anlagen in the skeletal muscle while inducing nearly complete regeneration and reestablishment of normal muscle architecture. HO was markedly decreased in the presence of *amiR-RH6* or *ACVR1^{opt}*, but the therapeutic effect of *amiR-RH6* was highly variable compared to that of *amiR-RH6.ACVR1^{opt}* and *ACVR1^{opt}* (**Fig. 4c and d**). These results demonstrated that systemic delivery of AAV gene therapy at birth could prevent trauma-induced HO in *Acvr1$^{(R206H)KI}$* FOP mice and that combination gene therapy is more effective than *ACVR1^{opt}* expression or *ACVR1^{R206H}* allele-specific silencing alone.

Muscle injury in a mouse model of FOP has been reported to induce the sequential pathological changes in HO lesion progression, including perivascular immune cell infiltration (Day 1-3), muscle degeneration and fibroproliferative response (Day 3-7), chondrogenesis (Day 7-14), and osteogenesis with heterotopic bone marrow establishment (Day 14-28).[9,41,42] To define the stage at which *amiR-RH6.ACVR1^{opt}* acts in HO pathogenesis, radiography and histopathological evaluation of AAV-treated,

injured muscle were performed at various time points. 6 weeks after i.v. injection into *Acvr1*$^{(R206H)Fl}$;Cre-ER^{T2} neonates at P1, pinch injury/cardiotoxin injection was introduced to the gastrocnemius muscle three days post-injection of tamoxifen and HO pathogenesis was assessed at day 3, 7, 14, and 28 after muscle injury (**Extended Data Fig. 8f**). As expected, positive HO control muscle from EGFP control-treated *Acvr1*$^{(R206H)KI}$ FOP mice showed early injury responses at day 3, including muscle degeneration, immune cell infiltration, and fibroblast proliferation, while chondrogenic anlagen appeared at day 7, and began to transform into heterotopic bone with bone marrow at day 14. HO was fully developed at day 28 post-injury (**Fig. 4d-f**). By contrast, there was little to no cartilage or heterotopic bone formation in *amiR-RH6.ACVR1*^{opt}-treated muscle and fibroproliferative responses were markedly reduced at day 14, resulting in the nearly complete reestablishment of normal muscle architecture at day 28 (**Fig. 4d-f**). This corresponds to reduced levels of phosphorylated SMAD1/5 in the skeletal muscles treated with *amiR-RH6.ACVR1*^{opt} relative to control, suggesting a potent inhibitory effect of *amiR-RH6.ACVR1*^{opt} on aberrant activation of BMP signaling within the injured muscle of FOP mice (**Fig. 4f**). Notably, early injury responses at day 3, including infiltration of inflammatory macrophages/monocytes (F4/80) and mast cells (toluidine blue), muscle degeneration, and fibroproliferation, were relatively comparable between the skeletal muscles treated with control and *amiR-RH6.ACVR1*^{opt} (**Fig. 4f**). Likewise, 84 genes associated with inflammatory responses showed comparable expression patterns between control- and *amiR-RH6.ACVR1*^{opt}-treated muscles except for *Tnfsf13/April*, *IL-11*, and *Ccl22* (**Fig. 4g and h**). Tnfsf13/April is a key cytokine that promotes B cell development by protecting from apoptosis,[43] IL-11 is an IL-6 family member that contributes to hematopoiesis, bone development, tissue repair, and tumor development,[44] and Ccl22 is a macrophage-derived chemokine that recruits TH2 cells into the inflammatory sites and the regulation of TH2-related immune responses.[45] Further studies will be necessary to define the contribution of these factors to trauma-induced HO in FOP mice. Consistent with our *in vitro* data showing the ability of *amiR-RH6.ACVR1*^{opt} to suppress Activin A-induced aberrant BMP signaling, chondrogenesis, and osteogenesis of human FOP iPSCs (**Fig. 2e-g**) and mouse *Acvr1*$^{(R206H)KI}$ skeletal progenitors (**Fig. 2h and I, 3a-e**), these results demonstrate that i.v.

administration of rAAV9.*amiR-RH6.ACVR1*^{opt} at birth prevented trauma-induced development of heterotopic endochondral ossification in *Acvr1*$^{(R206H)KI}$ FOP mice but showed minimal effects on early post-traumatic injury responses. Thus, systemic delivery of combination AAV gene therapy at birth is a promising approach to preventing trauma-induced HO in FOP mice at early adulthood.

AAV gene therapy given at birth prevents spontaneous HO in juvenile *Acvr1*$^{(R206H)KI}$ FOP mice

Since PDGFRα^{+} FAP-lineage cells in the skeletal muscle interstitium are a major cell of origin thought to be responsible for HO[9,37], mice harboring a conditional knock-in allele of *Acvr1*$^{(R206H)Fl}$ were crossed with PDGFRα-cre mice (*Acvr1*$^{(R206H)Fl}$*;PDGFRα-cre*), resulting in early-onset and widely distributed HO phenotypes of the musculature, tendons, and ligaments at multiple anatomical locations, including cervical spine, jaw, forelimb, hindlimb, hip and ankle (**Extended Data Fig. 9a**)[11]. 3-week-old *Acvr1*$^{(R206H)Fl}$*;PDGFRα-cre* mice were i.v. injected with rAAV9 expressing LacZ and β-galactosidase expression in multiple HO lesions was assessed by histology two weeks post-injection. These results confirmed the effectiveness of systemically delivered rAAV9 to transduce HO-residing cells in the skeletal muscle, ligament, and tendon throughout the body (**Fig. 5a**, **Extended Data Fig. 9b**). We next tested whether a single dose of i.v. administration with the rAAV9 at birth can prevent spontaneous HO during skeletal development. P1 *Acvr1*$^{(R206H)Fl}$*;PDGFRα-cre* neonates were i.v. injected with rAAV9 carrying EGFP control, *amiR-RH6*, *ACVR1*^{opt}, or *amiR-RH6.ACVR1*^{opt} and a full phenotypic characterization of these mice, including the natural history of progressive HO, bone remodeling, rate of disease progression, and survival rate, was performed. Compared to control-treated WT littermate control mice (*Acvr1*^{WT}*;ctrl*) showing a 100% survival rate, control-treated *Acvr1*$^{(R206H)Fl}$*;PDGFRα-cre* mice (*Acvr1*^{R206H}*;ctrl*) displayed a significant reduction in survival rate: 19% at 5 weeks and 100% lethality by 8 weeks (**Fig. 5b**). This survival rate was substantially improved by treatment with *amiR-RH6.ACVR1*^{opt}*:* 93% at 5 weeks, 67% at 8 weeks. Treatment with *amiR-RH6* or *ACVR1*^{opt} also increased survival rate: 50% or 67% at 5 weeks, 17% or 25% at 8 weeks, respectively. Likewise,

control-treated FOP mice weighed an average of 59% less than littermate control WT mice, and weight loss was markedly ameliorated by the treatment with *amiR-RH6.ACVR1^{opt}* relative to *amiR-RH6* or *ACVR1^{opt}* alone (**Fig. 5c**). Intriguingly, the majority of control-treated FOP mice developed HO bilaterally at the temporomandibular joints (TMJ) by the age of 7 weeks old, failed to open their mouths, and died early due to starvation (**Fig. 5d and e, Extended Data Fig. 10a**), suggesting that jaw ankylosis is the primary reason for the reduced survival rate and substantial weight loss of *Acvr1$^{(R206H)Fl}$;PDGFRα-cre* mice. These phenotypes were also significantly ameliorated by treatment with *amiR-RH6.ACVR1^{opt}* while only mild improvement was seen in mice treated with *amiR-RH6* or *ACVR1^{opt}* alone (**Fig. 5b-e**). Thus, systemic delivery of *amiR-RH6.ACVR1^{opt}* at birth, not *amiR-RH6* or *ACVR1^{opt}* alone, almost completely prevented early-onset, spontaneous HO at the TMJs in juvenile FOP mice, resulting in an increase in survival rate and body weight.

Since osteoporosis is a clinical feature in many advanced FOP patients[46,13], bone mass and architecture in the lumbar vertebrae (L4) of AAV-treated *Acvr1$^{(R206H)Fl}$;PDGFRα-cre* mice were assessed by microCT and histology (**Fig. 5d and f**, **Extended Data Fig. 10b**). Control-treated FOP mice showed ~70% decrease in vertebral bone mass compared to littermate control WT mice, and this bone loss was prevented by systemic delivery of *amiR-RH6.ACVR1^{opt}* at birth, but not *amiR-RH6* or *ACVR1^{opt}* alone. Notably, fluorescence microscopy of *PDGFRα-EGFP* reporter mice demonstrated high expression of PDGFRα in osteoblasts and osteocytes within alveolar bone and dental pulp mesenchymal stem cells and odontoblasts within tooth (**Extended Data Fig. 10c**)[47]. Control-treated *Acvr1$^{(R206H)Fl}$;PDGFRα-cre* mice displayed low alveolar bone mass in both maxillary and mandibular bones. However, tooth morphology and dentin mass were largely normal in these mice, suggesting that the *ACVR1^{R206H}* mutation may not directly affect tooth development. Similar to vertebral bone, alveolar bone loss in FOP mice was also almost completely prevented by treatment with *amiR-RH6.ACVR1^{opt}* (**Fig. 5g, Extended Data Fig. 10d and e**). Further studies will be necessary to define the contribution of the *ACVR1^{R206H}* mutation to this process using a tooth specific Cre mouse line[48].

As previously reported[49,11], whole body microCT scanning and radiography of control-treated, 5-week old *Acvr1*$^{(R206H)FI}$*;PDGFRα* mice showed spontaneous HO at multiple anatomical locations, including cervical spine, jaw, forelimb, hindlimb, hip and ankle (**Fig. 5d and h, Extended Data Fig. 11a**). Remarkably, systemic delivery of *amiR-RH6.ACVR1*^{opt} at birth almost completely prevented the incidence and severity of spontaneous HO throughout the body. Spontaneous HO was also reduced by treatment with *amiR-RH6* or *amiR-RH6.ACVR1*^{opt} while *ACVR1*^{opt} treatment showed a slight discrepancy between spontaneous HO incidence and severity (**Fig. 5d, h, i**). Daily i.p. injections of 2 week old FOP mice with a retinoic acid receptor γ agonist (palovarotene) has been reported to cause untoward skeletal toxicities, including synovial joint overgrowth and growth plate deformity in the long bone[49]. As systemic delivery of rAAV9 at birth was not effective for transduction of chondrocytes in the growth plates (**Extended Data Fig. 8c**), a single dose of i.v. injection with *amiR-RH6.ACVR1*^{opt} at birth did not perturb the development of proliferating and hypertrophic chondrocytes in the growth plate and articular cartilage (**Fig. 5j**, **Extended Data Fig. 11a**). Thus, unlike palovarotene that requires daily dosing and shows potential side effects, a single dose of systemic delivery of rAAV9.*amiR-RH6.ACVR1*^{opt} at birth is sufficient to prevent early onset, spontaneous HO in *Acvr1*$^{(R206H)KI}$ FOP mice without disturbing cartilage development.

Finally, to visualize how *amiR-RH6.ACVR1*^{opt} treatment prevents the pathogenesis of spontaneous HO in FOP mice, *Acvr1*$^{(R206H)FI}$*;PDGFRα-cre* mice were further crossed with *PDGFRα*-GFP reporter mice and P1 *Acvr1*$^{(R206H)FI}$*;PDGFRα-cre;PDGFRα-GFP* (*PDGFRα-GFP;Acvr1*^{R206H}) mice were i.v. injected with rAAV9 carrying mCherry control or *amiR-RH6.ACVR1*^{opt}. Five weeks later, *PDGFRα*$^{+}$ FAPs in the skeletal muscle were monitored by fluorescence microscopy using GFP expression (**Fig. 5k**). As expected, a subset of GFP-expressing *PDGFRα*$^{+}$ FAPs expressed mCherry, confirming AAV's transduction to *PDGFRα*$^{+}$ FAPs within forming HO lesions. mCherry control-expressing *PDGFRα*$^{+}$ FAPs differentiated into heterotopic bone-forming osteoblasts and primarily resided within forming HO lesions. By contrast, little to no evidence of heterotopic bone or

chondrogenic anlagen in the skeletal muscle expressing *amiR-RH6.ACVR1^{opt}* (**Extended Data Fig. 11b**); GFP-expressing *PDGFRα*$^{+}$ FAPs were primarily present in muscle interstitium (**Fig. 5k**), similar to WT *PDGFRα*$^{+}$ FAPs (**Fig. 4a, right**). Thus, systemic delivery of *amiR-RH6.ACVR1^{opt}* at birth is likely to suppress the initiation process of spontaneous HO in the skeletal muscle. Our data demonstrate that with a single dose of i.v. injection at birth, rAAV9.*amiR-RH6.ACVR1^{opt}* almost completely prevents spontaneous HO during early skeletogenesis and trauma-induced HO at early adulthood. Overall mobility, activity levels, and body stature were also substantially ameliorated in these mice (**Movie 1**).

Early adulthood treatment with AAV gene therapy prevents spontaneous HO in adult *Acvr1$^{(R206H)KI}$* FOP mice

To examine tissue biodistribution of systemically delivered rAAV9 during early adulthood in *Acvr1$^{(R206H)KI}$* FOP mice, 6-week-old *Acvr1$^{(R206H)Fl}$;*Cre-ER^{T2} mice were i.v. injected with rAAV9.*mCherry* three days after tamoxifen treatment. 12 weeks later, mCherry expression in the heart, kidney, liver, and skeletal muscle and knockdown efficiency of *ACVR1^{R206H}* and expression of *ACVR1^{opt}* in the liver were validated (**Fig. 6a, Extended Data Fig. 12a and b**). Alternatively, these mice were i.v. injected with a single dose of rAAV9.*amiR-RH6.ACVR1^{opt}* and 12 weeks later, control-treated *Acvr1$^{(R206H)Fl}$;*Cre-ER^{T2} mice progressively developed osteochondromas in the tibia, osteoarthritis in the knees, and spontaneous HO at multiple anatomical locations, including the cervical spine, hips and knees – skeletal features that are commonly seen in individuals with FOP[50]. Systemic delivery of *amiR-RH6.ACVR1^{opt}* at early adulthood prevented spontaneous HO from the cervical spine (**Fig. 6b and c**), while total HO mass and incidence throughout the body were substantially reduced in these mice (**Fig. 6d-f**). Additionally, control-treated mice often developed HO bridging the femur to the fibular head (**Fig. 6g, Movie 2 and 3**) and severe osteoarthritis in the knees (**Fig. 6h**), resulting in immobility of hindlimbs in *Acvr1$^{(R206H)KI}$* FOP mice. Thus, *Acvr1$^{(R206H)Fl}$;*Cre-ER^{T2} mice resemble multiple clinical FOP features found in human FOP patients, including progressive HO, orthotopic fusion of cervical vertebrae, fusion

of thoracic and lumbar vertebrae, osteochondromas, and early onset degenerative joint disease[50], which were all substantially prevented by the treatment with *amiR-RH6.ACVR1^{opt}* (**Fig. 6i**). Accordingly, these mice displayed normal mobility, activity levels, and body posture (**Movie 4**). Moreover, tissue morphology and structure in *amiR-RH6.ACVR1^{opt}*-treated mice are largely normal, suggesting little to no obvious anatomic off-target side effects of rAAV9.*amiR-RH6.ACVR1^{opt}* in non-HO tissues of FOP mice (**Extended Data Fig. 12c**). Previous studies demonstrated that BMP signaling plays critical roles in skeletal growth, joint patterning, and cartilage development during skeletogenesis, and that dysregulated BMP signaling by the *ACVR1^{R206H}* mutation disturbs these procedures.[39,51] However, tamoxifen treatment of *Acvr1$^{(R206H)Fl}$;*Cre-ER^{T2} mice at early adulthood did not develop any apparent abnormalities in growth plates in the presence of control or *amiR-RH6.ACVR1^{opt}* (**Fig. 6h**), suggesting minimal effects of the *ACVR1^{R206H}* mutation on the development of growth plates during early adulthood.

FOP patients have chronically elevated levels of hyper-inflammatory immune cells and pro-inflammatory cytokines[33,52,53]. FOP macrophages and mast cells are primed toward inflammatory responses[54], and depletion of these cells reduces HO in mice[42]. To examine the potential impact of i.v. injected rAAV9.*amiR-RH6.ACVR1^{opt}* on systemic immunity in *Acvr1$^{(R206H)Kl}$* FOP mice, complete blood counts, flow cytometry for immune cells, and spleen histology were performed in 18-week-old *Acvr1$^{(R206H)Fl}$* (control) and *Acvr1$^{(R206H)Fl}$;*Cre-ER^{T2} mice treated with control or *amiR-RH6.ACVR1^{opt}*. The numbers of platelets and immune cells, including T cells, B cells, dendritic cells, monocytes, macrophages, and neutrophils in the plasma and spleen, were comparable between control- and *amiR-RH6.ACVR1^{opt}*-treated mice (**Fig. 6j, Extended Data Fig. 13a and b**). Likewise, there was little to no alteration of germinal center architecture in AAV-treated spleens (**Extended Data Fig. 13c**). These results suggest that a single dose of i.v. administered rAAV9.*amiR-RH6.ACVR1^{opt}* is a potent inhibitor of spontaneous HO in adult FOP mice but no grossly apparent effects on cellular or tissue components of the immune system. Taken together, an AAV-mediated combination gene therapy that executes

ACVR1^{R206H} allele-specific silencing and *ACVR1*^{opt} expression at birth or early adulthood is a promising approach to prevent disabling HO, providing the potential for clinical translation to FOP patients.

Discussion

More than 95% of FOP patients have a heterozygous, ACVR1^{R206H} activating mutation that promotes dysregulated BMP signaling and subsequent transformation of soft connective tissues to heterotopic bone. AAV gene therapy is attractive for treating patients with FOP, due to the highly recurrent genetic cause, the lifelong progression of the severe extraskeletal formation, and high burden of taking a lifelong medication. In this study, we developed three AAV-based gene therapy approaches for FOP, including dilution of ACVR1^{R206H} receptor by over-expression of WT ACVR1 receptor (gene replacement), *ACVR1*^{R206H} allele-specific silencing by an AAV-compatible artificial miRNA, and the combination of gene replacement and silencing. These approaches function as potent suppressors of Activin A-induced aberrant BMP signaling, chondrogenesis, and osteogenesis of human FOP iPSCs and mouse *ACVR1*$^{(R206H)KI}$ skeletal cells while selectively inhibiting and/or diluting aberrant BMP signaling by the *ACVR1*^{R206H} mutation. We have shown that both t.d. and i.v. administration of the rAAV9 serotype can target early- and late-stages of HO-inducing cells, including FAP-lineage cells and mature osteoblasts. Importantly, AAV9-mediated gene therapy is effective when introduced at birth and early adulthood and can suppress both traumatic and spontaneous HO without causing detrimental effects on cartilage development, bone growth, or bone remodeling. Thus, our findings provide the first *in vivo* evidence that AAV-based gene therapy is a promising option for the prevention of HO in FOP.

In contrast to commercialized gene therapy for lipoprotein lipase deficiency[55], inherited retinal dystrophy[56], and spinal muscular atrophy[57], which introduces genes encoding missing proteins or encoding corrective proteins, our gene therapy approaches for FOP were designed to 1) dilute dysregulated BMP signaling effect of the mutant ACVR1^{R206H} receptor with the WT ACVR1 receptor, 2) silence the expression of the ACVR1^{R206H} receptor at the mRNA level using *ACVR1*^{R206H} allele-specific

amiR, or 3) remove the effects of the ACVR1^{R206H} receptor and express WT ACVR1 receptors simultaneously (**Extended Data Fig. 1**). While the therapeutic effects of these three approaches on trauma-induced HO were comparable in FOP mice with t.d. administration, when systemically delivered at birth, the combination gene therapy was most effective in suppressing both traumatic and spontaneous HO. This discrepancy may result from lower transduction efficiency of rAAV9 to targeted tissues via systemic delivery than direct local delivery. Alternatively, differential expression levels of ACVR1^{R206H} vs. ACVR1^{WT} within forming HO lesions at different anatomical locations may affect the therapeutic efficacy of these three different approaches on spontaneous HO in *ACVR1$^{(R206H)KI}$* FOP mice. Nonetheless, further studies will be necessary to define the stoichiometry of ACVR1^{R206H} and WT ACVR1 receptors in AAV-treated HO lesions and the long-term therapeutic outcomes of AAV gene therapy at different doses in preventing both traumatic and spontaneous HO in *ACVR1$^{(R206H)KI}$* FOP mice. Finally, correction of the classic *ACVR1^{R206H}* mutation (c.617G>A) at the genomic level using the clustered regularly interspaced short palindromic repeats (CRISPR)/Cas9-based adenine base editor (ABE) system was considered for FOP treatment by directly converting adenine to guanine in the human *ACVR1^{R206H}* allele without creating double-stranded DNA breaks[58]. However, it is challenging to use an AAV-based CRISPR/ABE system as *in vivo* gene therapy for FOP because ABE is a large bacteria-derived protein that exceeds the AAV packaging size limit (~4.7kb), and this system has low gene editing efficiency and high immunogenicity.

Our data demonstrate for the first time that the rAAV9 serotype is a highly effective vector for transducing FAP-lineage cells and osteoblasts within forming HO lesions. Accordingly, rAAV9-mediated gene therapy suppressed HO in *ACVR1$^{(R206H)KI}$* FOP mice when administered t.d. at early adulthood or i.v. at birth. Notably, despite a high transduction efficiency of the rAAV6.2 serotype in human and mouse osteogenic cells *in vitro*, rAAV6.2 was not effective for *in vivo* transduction of FAPs and osteoblasts in forming HO lesions. This discrepancy may be due to multiple physiological barriers, including the route of administration, serum factors, circulating neutralizing antibodies, and trans-vascularity[25]. rAAV9-mediated gene therapy is currently the leading platform for treating neurological

and musculoskeletal disorders, such as Parkinson's disease[59], amyotrophic lateral sclerosis (ALS)[60], type 1 spinal muscular atrophy (SMA)[61], and Duchenne muscular dystrophy (DMD)[62], in part, due to rAAV9's ability to target the central nervous system (CNS) and skeletal muscle when i.v. administered[63-64]. Previous studies have demonstrated that activating mutations in the human ACVR1 receptor that cause FOP, including the *ACVR1*^{R206H} mutation (c.617G>A)[4], are also involved in the tumorigenesis of diffuse intrinsic pontine glioma (DIPG)[65,66]. However, the activating mutations of ACVR1 in FOP are germline driving mutations whereas in DIPG, they are somatic within the tumor and are not associated with HO. DIPG is a pediatric brain tumor with a highly infiltrative malignant glial neoplasm of the ventral pons. The median survival time is 9–12 months, but neither surgical resection nor chemotherapeutic agents show any substantial survival benefit in clinical trials. Since treatment with ACVR1 inhibitors markedly prolonged the survival of DIPG mice[67-69], brain-transducible AAV9-mediated gene therapy for FOP might be also useful to treat tumorigenesis of DIPG. Further studies are needed to define the transduction efficiency of rAAV9 in the ventral pons and the therapeutic effects of rAAV9 vectors in DIPG mice with the *ACVR1*^{R206H} mutation. Since this study mainly focused on HO in *ACVR1*$^{(R206H)KI}$ FOP mice, effects of AAV gene therapy on non-HO phenotypes in FOP may not be addressed. Additionally, adult *Acvr1*$^{(R206H)Fl}$;Cre-ER^{T2} mice with tamoxifen-induced expression of *ACVR1*^{R206H} receptor after skeletal development may not recapitulate developmental aspects of FOP contributing to later HO phenotypes. Finally, since *Acvr1*$^{(R206H)Fl}$*;PDGFRα-cre* and tamoxifen-induced *Acvr1*$^{(R206H)Fl}$;Cre-ER^{T2} mice express *ACVR1*^{R206H} receptor only in a subset of HO-causing cells, these mouse models may not fully recapitulate HO phenotypes seen in patients with FOP.

Our proof-of-concept studies demonstrate AAV gene therapy is a potent inhibitor of traumatic and spontaneous HO in FOP mice, providing a potential clinical translation to FOP patients. However, since immunological triggers are known to pose a high risk for HO induction in FOP patients, any consideration of AAV gene therapy needs to be scrupulously approached. Although rAAVs have low post-infection immunogenicity[15], and FOP mice showed little to no immune responses to systemically delivered AAVs, a high dose administration of rAAVs could potentially induce systemic immune

responses in FOP patients complicating reliable delivery of therapeutic genes to HO-causing cells and may compromise the subsequent safety of this method as well as any therapeutic benefit. A cocktail therapy of rAAVs with immunosuppressors, FOP inhibitors, and/or non-immunogenic liposomes or nanoparticles might minimize FOP-associated immune responses. Alternatively, AAV capsid-specific chimeric antigen receptor-expressing regulatory T cells (AAV-CAR Tregs) have been shown to suppress immune responses to AAV capsids and transgenes[70], and might be engineered for AAV gene therapy for FOP. Further vector improvements to limit AAV expression in non-HO tissues and/or to specifically deliver therapeutic genes to HO-causing cells may address these issues. Finally, long-term durability and safety of therapeutic gene expression are of paramount importance in considering these approaches for potential use in FOP patients where lifelong HO suppression will be necessary. Clearly, future investigation for vector biodistribution, toxicity, and dose-ranging in large animals is required before any consideration can be given to applying AAV gene therapy to individuals who have FOP.

Methods

Plasmids

To screen human ACVR1^{R206H}-specific amiRs, endogenous complementary DNA sequences of human *ACVR1^{R206H}, ACVR1^{WT},* or *ACVR1^{opt}* were inserted into 3-UTR of the Renilla luciferase gene of pcDNA3 RLUC POLIRES FLUC (Addgene, #45642, **Extended Data Figure. 2a**). Mammalian expression vectors (pcDNA6) encoding human *ACVR1^{WT}* and *ACVR1^{R206H}* ORF were obtained from Dr. Hyun-Mo Ryoo (Seoul National University, **Extended Data Figure. 2b**).[71]

rAAV vector design and production

The pAAVsc-*CB6*-ACVR1^{opt} was generated by replacing the *mCherry* reporter with a codon-optimized version of the human ACVR1 complementary DNA (*ACVR1^{opt}*), and then, the chicken β actin (CBA) intron in the plasmid was replaced with the MassBiologics (MBL) or synthetic intron to reduce the AAV vector genome size (**Fig. 1a**). The artificial miRNA (amiR) against human *ACVR1^{R206H}* was designed by using a custom Excel macro, which considers miR-33 scaffold design rules to generate optimized amiR cassettes. The tool will be shared upon request. Plasmids were constructed by Gibson assembly and standard molecular biology methods. DNA sequences for *amiR-33-ctrl* and *amiR-33-human ACVR1^{R206H}* were synthesized as gBlocks and cloned into the intronic region of the pAAVsc-*CB6-mCherry* plasmid at the restriction enzyme sites (PstI and BglII, **Fig. 1c**)[72]. Constructs were verified by sequencing. Additionally, the pAAVsc-CB6-*Egfp* construct was packaged into AAV1 (1.8E+13 GC/ml), AAV2 (1.5E+12 GC/ml), AAV2TM (1.5E+12 GC/ml), AAV3 (6E+12 GC/ml), AAV4 (6.5E+12 GC/ml), AAV5 (2.4E+13 GC/ml), AAV6 (8E+12 GC/ml), AAV6.2 (8E+12 GC/ml), AAV7 (1.5E+13 GC/ml), AAV8 (7E+12 GC/ml), AAV9 (1.5E+13 GC/ml), AAVrh8 (8E+12 GC/ml), AAVrh10 (8E+12 GC/ml), AAVrh39 (1.0E+13 GC/ml), and AAVrh43 (6E+12 GC/ml) capsids. Alternatively, the constructs of pAAVsc-CB6.*mCherry* or pAAVsc-CB6.*LacZ* were packaged into AAV6.2 (1.0E+13 GC/ml) or AAV9 (1.0E+13 GC/ml) capsids. rAAV production was performed by transient transfection of HEK293 cells, purified by CsCl sedimentation, titered by droplet digital PCR (ddPCR) on a QX200

ddPCR system (Bio-Rad) using the *Egfp or mCherry* prime/probe set as previously described[73]. The sequences of gBlocks™ and oligonucleotides for ddPCR are listed in **Extended Data Table 1**.

Cell culture and reagents

HEK293T cells and C2C12 cells were purchased from ATCC and human bone marrow-derived mesenchymal stromal cells (BMSCs) were purchased from ScienCell Research Laboratories. They were cultured according to the manufacturers' manuals. Human adipose tissue-derived stromal cells (ASC) were kindly gifted from Dr. Silvia Corvera (UMass Chan Medical School) and cultured as described in the previous publications[28,29]. Induced pluripotent stem cells (iPSC) were generated from dermal fibroblasts of healthy human donors (WT) or FOP patients by Dr. Edward Hsiao (UCSF) and cultured as described in the previous publications[26,27]. Mouse fibroadipogenic progenitors (FAPs) were FACS sorted from the digested skeletal muscle of 4-week-old *Acvr1$^{(R206H)Fl}$;PDGFR*α-cre mice using cell surface markers (PDGFRα^{+}Sca1^{+}CD31^{-}CD45^{-}) and cultured as previously described[11]. Mouse bone marrow-derived stromal cells (BMSCs) were isolated from 4-week-old *Acvr1$^{(R206H)Fl}$* or *Acvr1$^{(R206H)Fl}$;PRRX1-cre* femurs. Cells were maintained in α-MEM medium (Gibco) containing 10% FBS (Corning), 2 mM L-glutamine (Corning), 1% penicillin/ streptomycin (Corning), and 1% nonessential amino acids (Corning) while they were differentiated into mature osteoblasts under osteogenic medium containing ascorbic acid (200 uM, Sigma, #A8960) and β-glycerophosphate (10 mM, Sigma, G9422). Mouse chondrogenic precursors were isolated from the knee joints of P2 *Acvr1$^{(R206H)Fl}$;PRRX1-cre* neonates using collagenase D (Sigma #11088866001) and cultured in DMEM (Corning) containing 10% FBS (Corning), 2 mM L-glutamine (Corning) and 1% penicillin/ streptomycin (Corning) as previously described[74]. Recombinant BMP4 (#314-BP), BMP2/7 (#3229-BM), and Activin A (#338-AC) proteins were purchased from R&D systems.

Mice

Acvr1$^{(R206H)Fl}$ mice[75] were kindly gifted from the International FOP Association and maintained on C57BL/6J background. *Cre-ER*^{T2}, *Pdgfrα-Cre*, and *Prrx1-Cre* mice were purchased from Jackson Laboratory and crossed with *Acvr1*$^{(R206H)Fl}$ mice to obtain *Acvr1R*$^{(R206H)Fl}$*;Cre-ER*^{T2}, *Acvr1R*$^{(R206H)Fl}$*;Pdgfrα-cre*, and *Acvr1R*$^{(R206H)Fl}$*;Prrx1-cre* mice, respectively, and maintained on C57BL/6J background. To label Pdgfrα-expressing FAPs, *Acvr1R*$^{(R206H)Fl}$*;Pdgfrα-cre* mice were further crossed with *Pdgfrα-GFP* reporter mice (Jackson Laboratory, C57BL/6J). To label Tie2-expressing FAPs, *Tie2-cre* mice (Jackson Laboratory, C57BL/6J) were crossed with Ai9-mCherry mice (Rosa26^{mCherry}, Jackson Laboratory). For postnatal activation of Cre-ER^{T2}, 100 mg/kg tamoxifen (Sigma, #T5648) in sunflower seed oil (Sigma, #S5007) was intraperitoneally (i.p.) injected to 6-week-old mice once a day for 5 consecutive days. Mouse genotypes were determined by PCR using tail genomic DNA. Primer sequences are available upon request. Control littermates were used and analyzed in all experiments. All animals were used in accordance with the NIH Guide for the Care and Use of Laboratory Animals and were handled according to protocols approved by the University of Massachusetts Chan Medical School Institutional Animal Care and Use Committee (IACUC).

MicroCT and radiography

MicroCT (uCT35; SCANCO Medical AG; Bruttisellen, Switzerland) was used for qualitative and quantitative assessment of trabecular and cortical bone microarchitecture and performed by an investigator blinded to the genotypes of the animals under analysis. MicroCT scanning was performed at 55 kVp and 114 mA energy intensity with 300-ms integration time. Specific voxel size used for femur, maxilla and mandibular body is 7 μm and 12 μm for vertebrae. All images were reconstructed using image matrices of 1024 X 1024 pixels. For trabecular bone analysis of the distal femur, an upper 2.1 mm region beginning 280 μm proximal to the growth plate was contoured. For the cortical bone analysis of femurs, a midshaft region of 0.6 mm in length was used. L4 spinal segments were used for vertebrae analysis. 3D reconstruction images were obtained from contoured 2D images by methods

based on distance transformation of the binarized images. Alternatively, the Inveon multimodality 3D visualization program was used to generate fused 3D viewing of multiple static or dynamic volumes of microCT modalities (Siemens Medical Solutions USA, Inc). All images presented are representative of the respective genotypes (n > 5).

Trident Specimen Radiography system (Hologic, USA) was used to generate detailed radiographic images of the whole mouse body after euthanasia. The X-ray beam intensity was 1 mA 28 kv ~ 30 KV with AEC (automatic exposure control) for fast image acquisition.

Histology and immunohistochemistry

For histological analysis, femurs, vertebrae, and skulls were dissected from AAV-treated mice, fixed in 10% neutral buffered formalin for two days at room temperature, and decalcified by 14% EDTA tetrasodium salt, pH 7.6 for 3 - 4 weeks at 4°C. Samples were kept in 70% ethanol until processed on a vacuum infiltration tissue processor. Sections were done on a microtome (HistoCore Multicut; Leica, USA) at a thickness of 6 µm along the coronal plate from anterior to posterior. Slides were stained with hematoxylin and eosin (H&E), alcian blue hematoxylin-orange G, or toluidine blue.

For immunohistochemistry, paraffin sections were dewaxed and stained following the manufacturer's procedure using the Discovery XT automated immunohistochemistry stainer (Ventana Medical Systems, Inc., Tucson, AZ, USA). Citrate-based antigen unmasking solution (Vector Laboratories, H-3300) and BLOXALL endogenous blocking solution (Vector laboratories, SP-6000) were used for antigen retrieval and blocking, respectively. Sections were incubated with antibodies specific to F4/80 (Cell Signaling Technology #70076, 1:100), phospho-SMAD1/5 (Cell Signaling Technology # 9516, 1:100) for overnight at 4°C, and a secondary antibody of VisUCyte™ HRP Polymer antibodies for 40 min at room temperature, then incubated with the substrate working solution (DAB substrate kit, Vector Sk-4100) at room temperature for 1- 2 minutes followed by hematoxylin staining (Vector laboratories H-3404). Reaction buffer (pH 7.6 Tris buffer) was used as a washing solution. The

stained samples were visualized either using an Olympus microscope Bx50 (Olympus, USA) or EVOS M7000 (Life technology, USA).

For frozen sectioning, dissected specimens were fixed in 4% paraformaldehyde for 2 ~3 days followed by 15 days of semi-decalcification using 14% EDTA tetrasodium salt, pH 7.6 at 4°C. Infiltration were processed using 20% sucrose solution prior to OCT embedding. Slides were prepared on Cryostat (LM3050s; Leica USA) at a thickness of 12 μm.

Quantitative RT-PCR, RT^2 profiler PCR arrays, and immunoblotting

The total RNA was purified from cells and tissues using QIAzol (QIAGEN) and cDNA was synthesized using the High-Capacity cDNA Reverse Transcription Kit (Applied Biosystems, #4368814). Quantitative RT-PCR was performed using iTaq™ Universal SYBR® Green Supermix (Bio-Rad, #1725122) with CFX connect RT-PCR detection system (Bio-Rad). To measure mRNA levels of the indicated genes in the injured areas or HO lesions of AAV-treated mice, the tibialis muscles were snap-frozen in liquid nitrogen for 30 sec and in turn homogenized in 1 ml of QIAzol for 1 min. Alternatively, HEK293T cells, human WT or FOP iPSCs, mouse FAPs, and osteogenic or chondrogenic progenitors were lysed using QIAzol and total RNA was subjected for RT-PCR analysis. Primers used for PCR are described in the **Extended Data Table 1.** Finally, RT^2 profiler PCR arrays (QIAGEN) were used to measure mRNA levels of 84 inflammatory cytokines and receptors, including *Ccl1, Ccl11, Ccl12, Ccl17, Ccl19, Ccl2, Ccl20, Ccl22, Ccl24, Ccl3, Ccl4, Ccl5, Ccl6, Ccl7, Ccl8, Ccl9, Cx3cl1, Cxcl1, Cxcl10, Cxcl11, Cxcl12, Cxcl13, Cxcl15, Cxcl5, Cxcl9, Ccr1, Ccr10, Ccr2, Ccr3, Ccr4, Ccr5, Ccr6, Ccr8, Cxcr2, Cxcr3, Cxcr5, Il11, Il13, Il15, Il16, Il17a, Il17b, Il17f, Il1a, Il1b, Il1rn, Il21, Il27, Il3, Il33, Il4, Il5, Il7, Il10ra, Il10rb, Il1r1, Il2rb, Il2rg, Il5ra, Il6ra, Il6st, Aimp1, Bmp2, Cd40lg, Csf1, Csf2, Csf3, Fasl, Ifng, Lta, Ltb, Mif, Nampt, Osm, Pf4, Spp1, Tnf, Tnfsf10, Tnfsf11, Tnfsf13, Tnfsf13b, Tnfsf4, Vegfa,* and *Tnfrsf11b*.

Cells were lysed in TNT lysis buffer (150 mM NaCl, 1% Triton X-100, 1 mM EDTA, 1 mM EGTA, 50 mM NaF, 1 mM Na_3VO_4, 1 mM PMSF and protease inhibitor cocktail (Sigma)) and protein amounts from cell lysates were measured using DC protein assay (Bio-Rad). Equivalent amounts of proteins

were subjected to SDS-PAGE, transferred to Immobilon-P membranes (Millipore), immunoblotted with anti-ACVR1 antibody (1:1000, Sigma #SAB3500435), anti-GAPDH antibody (1:1000, EMD Millipore #CB1001), anti-phospho-SMAD1/5 antibody (1:1000, Cell Signaling Technology # 9516), anti-GFP antibody (1:1000, Takara, #632381), anti-HSP90 antibody (1:1000, BioLegend, #675402), and developed with ECL (ThermoFisher Scientific). Immunoblotting with anti-HSP90 antibody or anti-GAPDH antibody was used as a loading control.

***In vitro* transduction assay of rAAV serotypes**

Human FOP iPSCs, BMSCs, or ASCs were plated at a density of 1 x 10^4 cells/well in 24-well plate and 24 hours later, they were incubated with rAAV1, rAAV2, rAAV2-TM, rAAV3, rAAV4, rAAV5, rAAV6, rAAV6.2, rAAV7, rAAV8, rAAV9, rAAVrh8, rAAVrh10, rAAVrh39, or rAAVrh43 vectors packaging the *CBA-Egfp* reporter transgene at three different titers (10^9-10^{11}/mL genome copies). 48 hours later, cells were washed with PBS and EGFP expression was monitored by the EVOS FL imaging system (ThermoFisher Scientific). Alternatively, cells were lysed in TNT lysis buffer and EGFP expression was assessed by immunoblotting with anti-EGFP antibody.

Osteoblast or chondrocyte differentiation analysis

To assess extracellular matrix mineralization in AAV-treated osteoblasts, cells were washed twice with 1X phosphate-buffered saline (PBS) and fixed in 70% EtOH for 15 min at room temperature. Fixed cells were washed twice with distilled water and then stained with 2% Alizarin red solution (Sigma, #A5533) for 5 min. Cells were then washed three times with distilled water and examined for the presence of calcium deposits. Mineralization was quantified by the acetic acid extraction method[76]. For alkaline phosphatase (ALP) staining, osteoblasts were fixed with 10% neutral buffered formalin and stained with the solution containing Fast Blue (Sigma, #FBS25) and Naphthol AS-MX (Sigma, #855). Alternatively, osteoblasts were incubated with 10-fold diluted Alamar Blue solution (Invitrogen, #DAL1100) for cell proliferation. Subsequently, cells were washed and incubated with a solution

containing 6.5 mM Na_2CO_3, 18.5 mM $NaHCO_3$, 2 mM $MgCl_2$, and phosphatase substrate (Sigma, #S0942), and ALP activity was measured by a spectrometer (BioRad).

To assess chondrogenic differentiation of AAV-treated chondrogenic progenitors, cells were washed with PBS and fixed with 4% glutaraldehyde for 15 min at room temperature. Fixed cells were washed with 0.1N HCL and stained with 1% alcian blue (Sigma, #A3157) for 30 min at room temperature. After washing with 0.1N HCL, stained proteoglycans in the extracellular matrix were detected as previously described[74].

Next-generation sequencing (NGS)

Transcripts of *ACVR1*^{WT} and *ACVR1*^{R206H} in AAV-treated human FOP iPSCs were quantitated by PCR amplicons using Next-Generation Sequencing (NGS). Briefly, 5 x 10^{10} GCs of the AAV6.2 vectors carrying EGFP control, *amiR-RH6.ACVR1*^{opt}, or *amiR-RH7.ACVR1*^{opt} were transduced to human FOP iPSCs for three days. The cDNAs synthesized from total RNA were amplified using ACVR1-targeting primers and the PCR products was subjected for NGS in the Massachusetts General Hospital Center for Computational & Integrative Biology DNA Core (Boston, MA).

Transcriptome analysis

RNA-seq samples were obtained from human FOP iPSCs treated with rAAV6.2 vector carrying EGFP contrl, *amiR-RH6.ACVR1*^{opt}, or *amiR-RH7.ACVR1*^{opt} and mapped to the human reference genome (GCF_000001405.38_GRCh38.p12) with STAR aligner (v.2.6.1b)[77,78]. After mapping, read counts were generated by using HTSeq-count (v.0.11.3)[79]. The read counts were used for a differential expression analysis between EGFP control (ctrl) vs. *amiR-RH6.ACVR1*^{opt}, EGFP control (ctrl) vs. *amiR-RH7.ACVR1*^{opt} and *amiR-RH6.ACVR1*^{opt} vs. *amiR-RH7.ACVR1*^{opt} using DESeq2 (v.1.28.1)[80] with the ashr shrinkage estimator (v.2.2.47)[81]. Genes with statistical significance were determined as having absolute log-fold change larger than 1.5 and having a P-value less than 0.005.

Complete blood cell count (CBC)

CBC tests were performed to evaluate cellular components in the blood of AAV-treated mice, including white blood cells (WBCs), red blood cells (RBCs), lymphocytes, monocytes, neutrophils, and platelets (PLTs). Blood drops were collected into a microtainer EDTA tube and tested within one hour at room temperature using an automated hematology analyzer (VetScan HM5, Zoetis.USA).

Flow cytometry for immune cell population

To isolate the splenocytes from AAV-treated mice, the spleens were quickly removed under aseptic conditions, then placed on wire mesh and gently teased with sterile forceps. Similarly, to isolate bone marrow cells, bone marrow was aspirated from mouse femurs of AAV-treated mice. Collected splenocytes and bone marrow cells were washed with 1 X Phosphate-buffered saline (PBS) and then incubated with RBC lysis buffer (BioLegend, #420301) for 2 - 5 min at room temperature to eliminate red blood cells (RBC). Further, cells were washed twice with cold fluorescence-activated cell sorting (FACS) buffer and filtered through sterile 40 μm cell strainer before resuspending into FACS buffer and then incubated with Fc blocking buffer (BD Biosciences, #564765) for 15 min at 4°C. After Fc receptor blocking, cells were treated with fluorochrome labelled antibody cocktail including anti-mouse/human CD11b APC (1:100, BioLegend, #101212), anti-mouse CD45R (B220) PerCP Cy 5.5 (1:100, Tonbo, #65-0452), anti-mouse CD3 FITC (1:100, BioLegend, #100203), anti-Mouse CD11c Brilliant Violet 510 (1:100, BioLegend, #117337), anti-mouse Ly6G PE-Cy7 (1:100, BioLegend, #127618) and anti-mouse Ly6C FITC (1:100, BioLegend, #128006) in cold FACS buffer. After treatment with Ghost Dye red 780 (1:1000, Tonbo, #13-0865-T100) for live/dead cell discrimination, cells were then subjected to acquisition on a BD LSR II flow cytometer (BD Biosciences). The data were analyzed using FlowJo (v.10.1).

Mouse models of acquired heterotopic ossification

5 x 10^{12} vector genomes vg/kg (50 µl) of rAAV6.2 or rAAV9 vectors were t.d. injected into the quadriceps muscle of 2-month-old wild-type or *Tie2-cre;Rosa26^{mCherry}* mice (C57BL/6J) using a hollow microneedle (micronjet600, NanoPass Technologies)[34] one week post-injection of rBMP2/7-matrigel and muscle injury, and three weeks later, radiography of hindlimbs and frozen sections of HO tissues were performed in AAV-treated mice. For muscle injury/BMP-induced HO model[35,36], blunt muscle trauma was induced by dropping an aluminum ball onto the mouse adductor muscle (right next to the femur) and a mixture of recombinant BMP2/7 (1 µg) and Matrigel (20 µl) was injected into the injured area. Subcutaneous injection of buprenorphine was provided for analgesia. Mice were euthanized and HO was assessed by radiography, microCT, and histology at four weeks post-injury.

Administration of rAAVs to *Acvr1R$^{(R206H)KI}$* FOP mice

Trauma-induced HO: 5 x 10^{12} vg/kg (50 µl) of rAAV9 vectors carrying CRE recombinase was t.d. injected into hindlimbs of 6-week-old *Acvr1R$^{(R206H)Fl}$* mice and three days later, 1 µM cardiotoxin/pinch injury was employed into AAV-injected sites. Alternatively, 6-week-old *Acvr1R$^{(R206H)Fl}$;*Cre-ER^{T2} mice were daily treated with intraperitoneal (i.p.) injection of tamoxifen (10 mg/kg) for five days and three days later, 5 x 10^{12} vg/kg (50 µl) of rAAV9 vectors carrying *mCherry, EGFP control, amiR-RH6, ACVR1^{opt}*, or *amiR-RH6.ACVR1^{opt}* was t.d. injected into hindlimbs. 1 µM cardiotoxin/pinch injury was employed into the gastrocnemius muscle three days after AAV injection. Finally, P1 *Acvr1R$^{(R206H)Fl}$;*Cre-ER^{T2} neonates were treated with 10^{11} GCs (50 µl) of rAAV9 carrying *mCherry, EGFP control, amiR-RH6, ACVR1^{opt}*, or *amiR-RH6.ACVR1^{opt}* via facial vein injection and six weeks later, mice were i.p. injected with tamoxifen (10 mg/kg), followed by 1 µM cardiotoxin/pinch injury of the gastrocnemius muscle three days after AAV injection. Four weeks later, *ACVR1^{R206H}* and *Cre* recombinase mRNA levels and heterotopic bone mass in the gastrocnemius muscle were assessed by RT-PCR, radiography, and microCT.

Spontaneous HO: P1 *Acvr1*$^{(R206H)Fl}$, *Acvr1*$^{(R206H)Fl}$;*PDGFR*α-cre, or *Acvr1*$^{(R206H)Fl}$;*PDGFR*α-cre;*PDGFR*α-GFP neonates were treated with 10^{11} GCs (50 µl) of rAAV9 carrying *mCherry, EGFP control, amiR-RH6*, *ACVR1*^{opt}, or *amiR-RH6.ACVR1*^{opt} via facial vein injection and a full phenotypic characterization was performed until mice were 8 weeks old. Alternatively, 6-week-old *Acvr1*$^{(R206H)Fl}$ or *Acvr1*$^{(R206H)Fl}$;*Cre-ER*^{T2} mice were i.v. administered 5 x 10^{13} vg/kg (200 µl) of rAAV9 carrying *EGFP control* or *amiR-RH6.ACVR1*^{opt} three days after i.p. injection of tamoxifen (10 mg/kg). 12 weeks later, mRNA levels of *ACVR1*^{R206H} and *ACVR1*^{opt} in the liver and HO were assessed by RT-PCR, microCT, radiography, and histology, respectively.

Clinical HO scoring

Euthanized mice were processed for whole body radiography and microCT analyses. Each mouse was independently scored by a minimum of two researchers, blinded as to the identity of the groups, and the average score was recorded. Clinical HO incidence or severity was calculated by adding the cumulative score of HO and skeletal deformity at all targeted sites per mouse. HO lesions and skeletal deformity were scored as mild (1), moderate (2), or severe (3) based on estimated size and fused condition at targeted sites (jaw;left/right, thoracic/cervical vertebrae, forelimb; left/right, hip, Knee; left/right, hindlimb; left/right and ankle; left/right).

Statistical Methods

All data were presented as the mean ± SD. Sample sizes were calculated on the assumption that a 30% difference in the parameters measured would be considered biologically significant with an estimate of sigma of 10-20% of the expected mean. Alpha and Beta were set to the standard values of .05 and 0.8, respectively. No animals or samples were excluded from analysis and animals were randomized to treatment versus control groups, where applicable. For relevant data analysis, where relevant, we first performed the Shapiro-Wilk normality test for checking normal distributions of the groups. If normality tests passed, two-tailed, unpaired Student's *t*-test was used and if normality tests

failed, and Mann-Whitney tests were used for the comparisons between two groups. For the comparisons of three or four groups, we used one-way ANOVA if normality tests passed, followed by Tukey's multiple comparison test for all pairs of groups. If normality tests failed, the Kruskal-Wallis test was performed and was followed by Dunn's multiple comparison test. The GraphPad PRISM software (v6.0a, La Jolla, CA) was used for statistical analysis. $P < 0.05$ was considered statistically significant. *, $P<0.05$; **, $P<0.01$; ***, $P<0.001$; and ****, $P<0.0001$.

Data availability

Data supporting the findings of this manuscript are available from the corresponding authors upon reasonable request.

References

1. Pignolo, R.J.*, et al.* Prevalence of fibrodysplasia ossificans progressiva (FOP) in the United States: estimate from three treatment centers and a patient organization. *Orphanet J Rare Dis* **16**, 350 (2021).
2. Kaplan, F.S.*, et al.* Fibrodysplasia ossificans progressiva. *Best Pract Res Clin Rheumatol* **22**, 191-205 (2008).
3. Shore, E.M. & Kaplan, F.S. Insights from a rare genetic disorder of extra-skeletal bone formation, fibrodysplasia ossificans progressiva (FOP). *Bone* **43**, 427-433 (2008).
4. Shore, E.M.*, et al.* A recurrent mutation in the BMP type I receptor ACVR1 causes inherited and sporadic fibrodysplasia ossificans progressiva. *Nat Genet* **38**, 525-527 (2006).
5. Hino, K.*, et al.* Neofunction of ACVR1 in fibrodysplasia ossificans progressiva. *Proc Natl Acad Sci U S A* **112**, 15438-15443 (2015).
6. Aykul, S.*, et al.* Activin A forms a non-signaling complex with ACVR1 and type II Activin/BMP receptors via its finger 2 tip loop. *Elife* **9**(2020).
7. Hatsell, S.J.*, et al.* ACVR1R206H receptor mutation causes fibrodysplasia ossificans progressiva by imparting responsiveness to activin A. *Sci Transl Med* **7**, 303ra137 (2015).
8. Alessi Wolken, D.M., Idone, V., Hatsell, S.J., Yu, P.B. & Economides, A.N. The obligatory role of Activin A in the formation of heterotopic bone in Fibrodysplasia Ossificans Progressiva. *Bone* **109**, 210-217 (2018).
9. Lounev, V.Y.*, et al.* Identification of progenitor cells that contribute to heterotopic skeletogenesis. *J Bone Joint Surg Am* **91**, 652-663 (2009).
10. Dey, D.*, et al.* Two tissue-resident progenitor lineages drive distinct phenotypes of heterotopic ossification. *Sci Transl Med* **8**, 366ra163 (2016).
11. Lees-Shepard, J.B.*, et al.* Activin-dependent signaling in fibro/adipogenic progenitors causes fibrodysplasia ossificans progressiva. *Nat Commun* **9**, 471 (2018).
12. Lees-Shepard, J.B. & Goldhamer, D.J. Stem cells and heterotopic ossification: Lessons from animal models. *Bone* **109**, 178-186 (2018).
13. Pignolo, R.J., Shore, E.M. & Kaplan, F.S. Fibrodysplasia ossificans progressiva: diagnosis, management, and therapeutic horizons. *Pediatr Endocrinol Rev* **10 Suppl 2**, 437-448 (2013).
14. Wentworth, K.L., Masharani, U. & Hsiao, E.C. Therapeutic advances for blocking heterotopic ossification in fibrodysplasia ossificans progressiva. *Br J Clin Pharmacol* **85**, 1180-1187 (2019).
15. Bulcha, J.T., Wang, Y., Ma, H., Tai, P.W.L. & Gao, G. Viral vector platforms within the gene therapy landscape. *Signal Transduct Target Ther* **6**, 53 (2021).
16. Yang, Y.S.*, et al.* Bone-Targeting AAV-Mediated Gene Silencing in Osteoclasts for Osteoporosis Therapy. *Mol Ther Methods Clin Dev* **17**, 922-935 (2020).
17. Yang, Y.S.*, et al.* Bone-targeting AAV-mediated silencing of Schnurri-3 prevents bone loss in osteoporosis. *Nat Commun* **10**, 2958 (2019).
18. Herzog, R.W. Encouraging and Unsettling Findings in Long-Term Follow-up of AAV Gene Transfer. *Mol Ther* **28**, 341-342 (2020).
19. Asokan, A., Schaffer, D.V. & Samulski, R.J. The AAV vector toolkit: poised at the clinical crossroads. *Molecular Therapy* **20**, 699-708 (2012).
20. Grimm, D.*, et al.* Fatality in mice due to oversaturation of cellular microRNA/short hairpin RNA pathways. *Nature* **441**, 537-541 (2006).
21. McBride, J.L.*, et al.* Artificial miRNAs mitigate shRNA-mediated toxicity in the brain: implications for the therapeutic development of RNAi. *Proceedings of the National Academy of Sciences of the United States of America* **105**, 5868-5873 (2008).
22. Xie, J.*, et al.* Effective and Accurate Gene Silencing by a Recombinant AAV-Compatible MicroRNA Scaffold. *Mol Ther* **28**, 422-430 (2020).
23. Li, M.*, et al.* High-efficiency transduction of fibroblasts and mesenchymal stem cells by tyrosine-mutant AAV2 vectors for their potential use in cellular therapy. *Hum Gene Ther* **21**, 1527-1543

(2010).
24. van Lieshout, L.P.*, et al.* A Novel Triple-Mutant AAV6 Capsid Induces Rapid and Potent Transgene Expression in the Muscle and Respiratory Tract of Mice. *Mol Ther Methods Clin Dev* **9**, 323-329 (2018).
25. Balakrishnan, B. & Jayandharan, G.R. Basic biology of adeno-associated virus (AAV) vectors used in gene therapy. *Curr Gene Ther* **14**, 86-100 (2014).
26. Barruet, E.*, et al.* The ACVR1 R206H mutation found in fibrodysplasia ossificans progressiva increases human induced pluripotent stem cell-derived endothelial cell formation and collagen production through BMP-mediated SMAD1/5/8 signaling. *Stem Cell Res Ther* **7**, 115 (2016).
27. Matsumoto, Y.*, et al.* Induced pluripotent stem cells from patients with human fibrodysplasia ossificans progressiva show increased mineralization and cartilage formation. *Orphanet J Rare Dis* **8**, 190 (2013).
28. Min, S.Y.*, et al.* Diverse repertoire of human adipocyte subtypes develops from transcriptionally distinct mesenchymal progenitor cells. *Proc Natl Acad Sci U S A* **116**, 17970-17979 (2019).
29. Rojas-Rodriguez, R.*, et al.* Generation of Functional Human Adipose Tissue in Mice from Primed Progenitor Cells. *Tissue Eng Part A* **25**, 842-854 (2019).
30. Barruet, E. & Hsiao, E.C. Application of human induced pluripotent stem cells to model fibrodysplasia ossificans progressiva. *Bone* **109**, 162-167 (2018).
31. Gregorevic, P.*, et al.* Systemic delivery of genes to striated muscles using adeno-associated viral vectors. *Nat Med* **10**, 828-834 (2004).
32. Goldstein, J.M.*, et al.* In Situ Modification of Tissue Stem and Progenitor Cell Genomes. *Cell Rep* **27**, 1254-1264 e1257 (2019).
33. Pignolo, R.J.*, et al.* The Natural History of Flare-Ups in Fibrodysplasia Ossificans Progressiva (FOP): A Comprehensive Global Assessment. *J Bone Miner Res* **31**, 650-656 (2016).
34. Heine, S.J.*, et al.* Intradermal delivery of Shigella IpaB and IpaD type III secretion proteins: kinetics of cell recruitment and antigen uptake, mucosal and systemic immunity, and protection across serotypes. *J Immunol* **192**, 1630-1640 (2014).
35. Liu, X.*, et al.* A novel mouse model of trauma induced heterotopic ossification. *J Orthop Res* **32**, 183-188 (2014).
36. Nozaki, M.*, et al.* Improved muscle healing after contusion injury by the inhibitory effect of suramin on myostatin, a negative regulator of muscle growth. *Am J Sports Med* **36**, 2354-2362 (2008).
37. Wosczyna, M.N., Biswas, A.A., Cogswell, C.A. & Goldhamer, D.J. Multipotent progenitors resident in the skeletal muscle interstitium exhibit robust BMP-dependent osteogenic activity and mediate heterotopic ossification. *J Bone Miner Res* **27**, 1004-1017 (2012).
38. Kaplan, F.S., Chakkalakal, S.A. & Shore, E.M. Fibrodysplasia ossificans progressiva: mechanisms and models of skeletal metamorphosis. *Dis Model Mech* **5**, 756-762 (2012).
39. Chakkalakal, S.A.*, et al.* An Acvr1 R206H knock-in mouse has fibrodysplasia ossificans progressiva. *J Bone Miner Res* **27**, 1746-1756 (2012).
40. Uezumi, A.*, et al.* Identification and characterization of PDGFRalpha+ mesenchymal progenitors in human skeletal muscle. *Cell Death Dis* **5**, e1186 (2014).
41. Kaplan, F.S.*, et al.* Hematopoietic stem-cell contribution to ectopic skeletogenesis. *J Bone Joint Surg Am* **89**, 347-357 (2007).
42. Convente, M.R.*, et al.* Depletion of Mast Cells and Macrophages Impairs Heterotopic Ossification in an Acvr1(R206H) Mouse Model of Fibrodysplasia Ossificans Progressiva. *J Bone Miner Res* **33**, 269-282 (2018).
43. Hahne, M.*, et al.* APRIL, a new ligand of the tumor necrosis factor family, stimulates tumor cell growth. *J Exp Med* **188**, 1185-1190 (1998).
44. Putoczki, T. & Ernst, M. More than a sidekick: the IL-6 family cytokine IL-11 links inflammation to cancer. *J Leukoc Biol* **88**, 1109-1117 (2010).
45. Vulcano, M.*, et al.* Dendritic cells as a major source of macrophage-derived chemokine/CCL22 in vitro and in vivo. *Eur J Immunol* **31**, 812-822 (2001).

46. Singh, S.*, et al.* Surgical management of bilateral hip fractures in a patient with fibrodysplasia ossificans progressiva treated with the RAR-gamma agonist palovarotene: a case report. *BMC Musculoskelet Disord* **21**, 204 (2020).
47. Xu, X., Bringas, P., Jr., Soriano, P. & Chai, Y. PDGFR-alpha signaling is critical for tooth cusp and palate morphogenesis. *Dev Dyn* **232**, 75-84 (2005).
48. Sreenath, T.L., Cho, A., Thyagarajan, T. & Kulkarni, A.B. Odontoblast-specific expression of cre recombinase successfully deletes gene segments flanked by loxP sites in mouse teeth. *Genesis* **35**, 94-99 (2003).
49. Lees-Shepard, J.B.*, et al.* Palovarotene reduces heterotopic ossification in juvenile FOP mice but exhibits pronounced skeletal toxicity. *Elife* **7**(2018).
50. Kaplan, F.S.*, et al.* Classic and atypical fibrodysplasia ossificans progressiva (FOP) phenotypes are caused by mutations in the bone morphogenetic protein (BMP) type I receptor ACVR1. *Hum Mutat* **30**, 379-390 (2009).
51. Towler, O.W., Peck, S.H., Kaplan, F.S. & Shore, E.M. Dysregulated BMP signaling through ACVR1 impairs digit joint development in fibrodysplasia ossificans progressiva (FOP). *Dev Biol* **470**, 136-146 (2021).
52. Barruet, E.*, et al.* NF-kappaB/MAPK activation underlies ACVR1-mediated inflammation in human heterotopic ossification. *JCI Insight* **3**(2018).
53. Pignolo, R.J.*, et al.* Plasma-Soluble Biomarkers for Fibrodysplasia Ossificans Progressiva (FOP) Reflect Acute and Chronic Inflammatory States. *J Bone Miner Res* (2021).
54. Matsuo, K.*, et al.* ACVR1(R206H) extends inflammatory responses in human induced pluripotent stem cell-derived macrophages. *Bone* **153**, 116129 (2021).
55. Carpentier, A.C.*, et al.* Effect of alipogene tiparvovec (AAV1-LPL(S447X)) on postprandial chylomicron metabolism in lipoprotein lipase-deficient patients. *The Journal of clinical endocrinology and metabolism* **97**, 1635-1644 (2012).
56. Chiu, W.*, et al.* An Update on Gene Therapy for Inherited Retinal Dystrophy: Experience in Leber Congenital Amaurosis Clinical Trials. *International journal of molecular sciences* **22**(2021).
57. Mendell, J.R.*, et al.* Five-Year Extension Results of the Phase 1 START Trial of Onasemnogene Abeparvovec in Spinal Muscular Atrophy. *JAMA neurology* **78**, 834-841 (2021).
58. Levy, J.M.*, et al.* Cytosine and adenine base editing of the brain, liver, retina, heart and skeletal muscle of mice via adeno-associated viruses. *Nat Biomed Eng* **4**, 97-110 (2020).
59. Blits, B. & Petry, H. Perspective on the Road toward Gene Therapy for Parkinson's Disease. *Front Neuroanat* **10**, 128 (2016).
60. Mueller, C.*, et al.* SOD1 Suppression with Adeno-Associated Virus and MicroRNA in Familial ALS. *N Engl J Med* **383**, 151-158 (2020).
61. Pattali, R., Mou, Y. & Li, X.J. AAV9 Vector: a Novel modality in gene therapy for spinal muscular atrophy. *Gene Ther* **26**, 287-295 (2019).
62. Kodippili, K.*, et al.* Dual AAV Gene Therapy for Duchenne Muscular Dystrophy with a 7-kb Mini-Dystrophin Gene in the Canine Model. *Hum Gene Ther* **29**, 299-311 (2018).
63. Foust, K.D.*, et al.* Intravascular AAV9 preferentially targets neonatal neurons and adult astrocytes. *Nat Biotechnol* **27**, 59-65 (2009).
64. Bish, L.T.*, et al.* Adeno-associated virus (AAV) serotype 9 provides global cardiac gene transfer superior to AAV1, AAV6, AAV7, and AAV8 in the mouse and rat. *Hum Gene Ther* **19**, 1359-1368 (2008).
65. Buczkowicz, P.*, et al.* Genomic analysis of diffuse intrinsic pontine gliomas identifies three molecular subgroups and recurrent activating ACVR1 mutations. *Nat Genet* **46**, 451-456 (2014).
66. Taylor, K.R.*, et al.* Recurrent activating ACVR1 mutations in diffuse intrinsic pontine glioma. *Nat Genet* **46**, 457-461 (2014).
67. Carvalho, D.*, et al.* ALK2 inhibitors display beneficial effects in preclinical models of ACVR1 mutant diffuse intrinsic pontine glioma. *Commun Biol* **2**, 156 (2019).
68. Williams, E. & Bullock, A.N. Structural basis for the potent and selective binding of LDN-212854

to the BMP receptor kinase ALK2. *Bone* **109**, 251-258 (2018).
69. Hoeman, C.M.*, et al.* ACVR1 R206H cooperates with H3.1K27M in promoting diffuse intrinsic pontine glioma pathogenesis. *Nat Commun* **10**, 1023 (2019).
70. Arjomandnejad, M.*, et al.* Modulating immune responses to AAV by expanded polyclonal T-regs and capsid specific chimeric antigen receptor T-regulatory cells. *Mol Ther Methods Clin Dev* **23**, 490-506 (2021).
71. Song, G.A.*, et al.* Molecular consequences of the ACVR1(R206H) mutation of fibrodysplasia ossificans progressiva. *J Biol Chem* **285**, 22542-22553 (2010).
72. Xie, J.*, et al.* Short DNA Hairpins Compromise Recombinant Adeno-Associated Virus Genome Homogeneity. *Mol Ther* **25**, 1363-1374 (2017).
73. Gao, G. & Sena-Esteves, M. Introducing genes into mammalian cells: Viral vectors. *Molecular Cloning* **2**, 1209-1313 (2012).
74. Gosset, M., Berenbaum, F., Thirion, S. & Jacques, C. Primary culture and phenotyping of murine chondrocytes. *Nat Protoc* **3**, 1253-1260 (2008).
75. Lyu, H., Elkins, C.M., Pierce, J.L., Serezani, C.H. & Perrien, D.S. MyD88 Is Not Required for Muscle Injury-Induced Endochondral Heterotopic Ossification in a Mouse Model of Fibrodysplasia Ossificans Progressiva. *Biomedicines* **9**(2021).
76. Gregory, C.A., Gunn, W.G., Peister, A. & Prockop, D.J. An Alizarin red-based assay of mineralization by adherent cells in culture: comparison with cetylpyridinium chloride extraction. *Anal Biochem* **329**, 77-84 (2004).
77. Dobin, A.*, et al.* STAR: ultrafast universal RNA-seq aligner. *Bioinformatics* **29**, 15-21 (2013).
78. Dobin, A. & Gingeras, T.R. Mapping RNA-seq Reads with STAR. *Curr Protoc Bioinformatics* **51**, 11 14 11-11 14 19 (2015).
79. Anders, S., Pyl, P.T. & Huber, W. HTSeq--a Python framework to work with high-throughput sequencing data. *Bioinformatics* **31**, 166-169 (2015).
80. Love, M.I., Huber, W. & Anders, S. Moderated estimation of fold change and dispersion for RNA-seq data with DESeq2. *Genome Biol* **15**, 550 (2014).
81. Stephens, M. False discovery rates: a new deal. *Biostatistics* **18**, 275-294 (2017).

Acknowledgements

We would like to thank Drs. Daniel Perrien and Silvia Corvera for providing *Acvr1*$^{(R206H)Fl}$ mice and human ASCs, respectively, and Eunhye Son, Oksun Lee, Zhihao Chen, and Samuel Kou for technical support, and the many individuals who provided valuable reagents. We also thank Drs. Marelise Eekhoff, Dimitra Micha, Paul Yu, Jeffrey Chamberlain, David Goldhamer, Benjamin Levi, Yuji Mishina, Adam Sherman and Danielle Kerkovich for thoughtful discussion. G.G. is supported by grants from the NIH (P01AI100263, R01NS076991, P01HD080642, R01AI12135). J.H.S. is supported by NIH/NIAMS (R21AR077557, R01AR078230), the International FOP Association, and AAVAA Therapeutics. F.S.K. is supported by the Isaac & Rose Nassau Professorship of Orthopaedic Molecular Medicine. E.M.S. is supported by the Cali/Weldon Professorship for FOP Research.

Author Contributions

Y.S.Y. and J.M.K. designed, executed, and interpreted the experiments. H.M. and J.X. designed and generated all of the AAVs. C.L. and S.C. analyzed dental/alveolar bone and immune responses in FOP mice, respectively. E.H. provided healthy and FOP patient-derived iPSCs and assisted with editing of the manuscript. J.H.H. and H.H.C. performed whole transcriptome analysis. F.S.K. and E.M.S. supervised the research and manuscript development. G.G. and J.H.S. supervised the research and prepared the manuscript. All authors revised the manuscript and approved the final draft.

Competing Interests

G.G. and J.H.S. have submitted a patent application concerning the methodology described in this study. G.G. and J.H.S. are scientific co-founders of AAVAA Therapeutics and hold equity in this company. G.G. is also a scientific co-founder of Voyager Therapeutics and Aspa Therapeutics and holds equity in these companies. G.G. is an inventor on patents with potential royalties licensed to Voyager Therapeutics, Aspa Therapeutics Inc., and other biopharmaceutical companies. E.C.H. serves in a volunteer capacity on the registry advisory board of the IFOPA; on the International Clinical Council

on FOP, and on the Fibrous Dysplasia Foundation Medical Advisory Board. E.C.H. received prior research support through his institution from Regeneron Pharmaceuticals. E.C.H. receives clinical trials research support through his institution from Clementia, an Ipsen company. F.S.K. is the founder and past-President of the International Clinical Council (ICC) on FOP. F.S.K. serves in a volunteer capacity on the registry advisory board of the IFOPA. F.S.K. is an investigator on clinical trials sponsored by Clementia, an Ipsen company and by Regeneron Pharmaceuticals. E.M.S. serves in a volunteer capacity as a research advisor to the IFOPA. These pose no conflicts for this study. Other authors declare no conflicts of interest.

Figure 1: Development of AAV vector targeting the human *ACVR1^{R206H}* receptor

a. Schematic diagram of the plasmids expressing a codon-optimized version of the human ACVR1 complementary DNA (*ACVR1^{opt}*) with the CBA promoter and three different introns. CBA: CMV enhancer/chicken β-actin promoter. **b.** Validation of the expression of the ACVR1^{opt} receptor. Plasmids expressing *ACVR1^{opt}* were transiently transfected into HEK293 cells and cell lysates were subjected to immunoblotting with anti-ACVR1 antibody. Anti-HSP90 antibody was used as a loading control. **c.** Schematic diagram representing 12 amiRs that target different sequence sites of human *ACVR1^{R206H}* mRNA (*amiR-ACVR1^{R206H}*). The red box indicates the R206H mutation site (c.617G>A). Adenine (green) was mismatched to increase the selectivity of gene silencing. **d.** Plasmids encoding *amiR-ctrl* or 12 different *amiRs* were transiently transfected into HEK293 cells along with amiR-sensor plasmids (sensor-Luc) that contain *Renilla* luciferase and aimR complimentary sequences for human ACVR1^{R206H}, ACVR1^{WT}, and ACVR1^{opt}. One day later, a luciferase assay was performed to measure *Renilla* luciferase and normalized to firefly luciferase. Lower activities indicate higher silencing efficacy of amiRs. **e.** Plasmids encoding *amiR-ctrl* or 12 different *amiRs* were transiently transfected into HEK293 cells along with a plasmid expressing human ACVR1^{R206H}, ACVR1^{WT}, or ACVR1^{opt} cDNA and immunoblotted for ACVR1. Anti-HSP90 antibody was used for loading control. **f.** Schematic diagram of the combination gene therapy constructs expressing *amiR-ACVR1^{R206H}* (RH6 or RH7) and *ACVR1^{opt}* cDNA under the CBA promoter and MBL intron (MBLi) or synthetic intron (Syni). **g, h.** Plasmids encoding *amiR-ctrl* (ctrl), Syni.amiR-RH6.ACVR1^{opt}, Syni.amiR-RH7.ACVR1^{opt}, MBLi.amiR-RH6.ACVR1^{opt}, or MBLi.amiR-RH7.ACVR1^{opt} were transiently transfected into HEK293 cells along with sensor-Luc plasmids. Luciferase assay **(g)** or immunoblotting analysis for ACVR1 **(h)** was performed. Anti-HSP90 antibody was used for loading control. **i.** Plasmids were transiently transfected into HEK293 cells along with the BMP SMADs-responsive reporter gene (BRE-luc) and treated with Activin A (100 ng/ml). 24 hours later, Activin A signaling activity was measured by luciferase assay. Values represent mean ± SD: *, $P < 0.05$ by an unpaired two-tailed Student's *t*-test or one-way ANOVA test (**i**).

Figure 2: Effects of AAV gene therapy in human FOP iPSCs and mouse *Acvr1*$^{(R206H)KI}$ cells

a. Human FOP iPSCs were treated with PBS or 5 x 10^{10} genome copies (GCs) of 15 different AAV capsids packaged with the same *CBA-Egfp* transgene. 2 days later, EGFP expression was assessed by immunoblotting with an anti-GFP antibody**.** Anti-HSP90 antibody was used for loading control. **b.** Genome integrity of rAAV6.2 carrying *amiR-RH6.ACVR1*^{opt} or *amiR-RH7.ACVR1*^{opt} was assessed by electrophoresis in native gel. ssFL: single-stranded full-length. **c, d.** 5 x 10^{10} GCs of rAAV6.2 carrying *EGFP control (ctrl), amiR-RH6.ACVR1*^{opt}, or *amiR-RH7.ACVR1*^{opt} were transduced to human FOP iPSCs, cultured under osteogenic conditions for 4 days, and subjected to next-generation sequencing (NGS) for ratio expression: *ACVR1*^{R206H} *vs. ACVR1*^{WT} (**c, top**) or RT-PCR for *ACVR1*^{opt} expression (**c, bottom**). Alternatively, total RNA was subjected to bulk RNA sequencing (**d**). A volcano plot showing the gene expression for up/downregulated genes in the cells expressing *amiR-RH6.ACVR1*^{opt} or *amiR-RH7.ACVR1*^{opt} relative to *control*-expressing cells is displayed. **e-g.** AAV-treated, human WT or FOP iPSCs were cultured under osteogenic conditions and alkaline phosphatase activity (ALP) and alizarin red staining were performed to assess early and late osteoblast differentiation, respectively (**e**). Alternatively, osteogenic gene expression (Runx2) was assessed by RT-PCR (**f**). AAV-treated, human FOP iPSCs were incubated with PBS or Activin A (100 ng/ml) for 6 hours, and *ID1* mRNA levels were measured by RT-PCR (**g**). **h, i.** PDGFRα^{+}Sca1^{+}CD31^{-}CD45^{-} FAPs were sorted by FACS from the digested skeletal muscle of 4-week-old *Acvr1*$^{(R206H)Fl}$*;PDGFR*α-cre mice and transduced with 5 x 10^{10} GCs of AAV6.2 carrying *EGFP control, amiR-RH6.ACVR1*^{opt}, or *amiR-RH7.ACVR1*^{opt}. 2 days later, AAV-treated FAPs were cultured under osteogenic conditions with PBS or Activin A (50 ng/ml) for 6 days, and ALP activity (**h**) and osteogenic gene expression (BGLAP, IBSP, **i**) were assessed for osteoblast differentiation. Values represent mean ± SD: ns, non-significant; *, P <0.05; **, P < 0.01; ***, P < 0.001; ****, P < 0.0001 by an unpaired two-tailed Student's t-test or one-way ANOVA test (**e-i**).

Figure 3: AAV gene therapy suppresses Activin A signaling and trauma-induced HO

a–d. *PRRX1*$^{+}$ osteogenic progenitors were isolated from the long bones of 4-week-old *PRRX1-cre* (*Acvr1*^{WT}) or *Acvr1*$^{(R206H)Fl}$*;PRRX1-cre* mice and transduced with 5 x 10^{10} GCs of AAV6.2 carrying *EGFP control, amiR-RH6, ACVR1*^{opt}, or *amiR-RH6.ACVR1*^{opt}. 2 days later, AAV-treated cells were stimulated with Activin A (100 ng/ml) for 30 min and immunoblotted for phospho-SMAD1/5. Anti-GAPDH antibody was used for loading control (**a**). 6 hours after Activin A stimulation*, Id1* mRNA levels were assessed by RT-PCR (**b**). AAV-treated cells were cultured under osteogenic conditions with PBS, Activin A (50 ng/ml, **c**), or BMP4 (50 ng/ml, **d**) for 12 days, and Alizarin red staining was performed to detect mineralization. **e.** *PRRX1*$^{+}$ chondrogenic progenitors were isolated from the knee joints of P2 *Acvr1*$^{(R206H)Fl}$*;PRRX1-cre* neonates, transduced with AAV6.2 carrying *EGFP control* or *amiR-RH6.ACVR1*^{opt}, and cultured under chondrogenic conditions for 4 or 6 days. *Aggrecan* mRNA levels or Alcian blue staining were performed for chondrogenesis assessment. **f.** 5 x 10^{12} vg/kg of rAAV9.*egfp* was t.d. injected into the quadricep of 2-month-old *Tie2-cre;Rosa26*^{mCherry} mice that label Tie^{+} FAPs and endothelial cells (red, n=3) using a hollow microneedle 1 week after i.m. injection with rBMP2/7/matrigel and muscle injury. 3 weeks later, radiography of hindlimbs and histology on frozen sections of HO tissues were performed to visualize GFP-expressing FAP-lineage cells. The red box indicates a heterotopic bone (HB) in the skeletal muscle. DAPI was used for nuclear staining. M, muscle; HB-BM, heterotopic bone-bone marrow. Scale bars: 5 mm, **left top**; 500 μm, **left bottom**; 400 μm, **right. g, h.** 5 x 10^{12} vg/kg of rAAV9 expressing vector control (Vec) or Cre recombinase was t.d. injected into the hindlimb of 6-week-old *Acvr1R*$^{(R206H)Fl}$ mice (n=8), and 1 μM cardiotoxin/pinch injury was introduced into the gastrocnemius muscle 3 days post-injection. 4 weeks later, mRNA levels of *ACVR1*^{R206H} and *Cre* recombinase were assessed by RT-PCR **(g)** and heterotopic bone volume was detected by radiography and quantified by microCT **(h).** 3D reconstruction images and quantification of HO volume are displayed. Scale bars: 5 mm, **left top**; 1 mm, **left bottom**. **i.** For trauma-induced HO in FOP mice, 5 x 10^{12} vg/kg of rAAV9 carrying *EGFP control, amiR-RH6, ACVR1*^{opt}, or *amiR-RH6.ACVR1*^{opt} was t.d. injected into the hindlimbs of 6-week-old *Acvr1R*$^{(R206H)Fl}$*;Cre-ER*^{T2} mice (n=8) 3 days post-injection of tamoxifen (10 mg/kg). A 1 μM cardiotoxin/pinch injury was applied to the gastrocnemius muscle 3 days

post-injection. 4 weeks later, HO was assessed by microCT. 3D reconstruction images and quantification of HO volume are displayed. Scale bar: 1 mm. **j.** For trauma-induced HO in WT mice, 5 x 10^{12} vg/kg of rAAV9 expressing *EGFP control* or *amiR-RH6.ACVR1^{opt}* was t.d. injected into the quadricep of 2-month-old WT mice (n=5) followed by an rBMP2/7/matrigel injection and a muscle injury. 4 weeks later, HO was assessed by radiography and microCT. 3D reconstruction images and quantification of HO volume are displayed**.** Scale bars: 5 mm, **top**; 1 mm, **bottom.** Values represent mean ± SD: ns, non-significant; *, $P < 0.05$; **, $P < 0.01$; ***, $P < 0.001$; and ****, $P < 0.0001$ by an unpaired two-tailed Student's t-test or one-way ANOVA test (**b-e, g-j**).

Figure 4: Systemic delivery of AAV gene therapy at birth prevents traumatic HO in FOP mice

a. P1 PDGFRα-GFP reporter neonates (n=3) were i.v. injected with 10^{11} GCs of rAAV9 expressing mCherry and 2 weeks later, mCherry and GFP expression in frozen sections of AAV-treated tibia and muscle was assessed by fluorescence microscopy. BM: bone marrow. Scale bars: 100 μm, **left**; 50 μm, **right**. **b-d.** P1 *Acvr1$^{(R206H)Fl}$;Cre-ER^{T2}* neonates (n=10) were i.v. injected with 10^{11} GCs of rAAV9 carrying *EGFP control, amiR-RH6, ACVR1^{opt}*, or *amiR-RH6.ACVR1^{opt}* and 6 weeks later, mice were treated with tamoxifen (10 mg/kg). A 1 μM cardiotoxin/pinch injury was applied to the gastrocnemius muscle 3 days post-tamoxifen treatment. 4 weeks later, mRNA levels of *ACVR1^{R206H}* and *ACVR1^{opt}* were measured by RT-PCR **(b)** and HO in the gastrocnemius muscle was assessed by microCT and histology **(c, d)**. 3D reconstruction images **(d)** and quantification of HO volume **(c)** are displayed**.** Alcian blue staining of HO tissues **(d)** was performed to assess chondrogenic anlagen. Scale bars: 1 mm, **top**; 200 μm, **bottom**. **e-h.** To investigate the progression of HO pathogenesis, P1 *Acvr1R$^{(R206H)Fl}$* or *Acvr1R$^{(R206H)Fl}$;Cre-ER^{T2}* neonates (n=3) were i.v. injected with 10^{11} GCs of rAAV9 carrying *EGFP control* or *amiR-RH6.ACVR1^{opt}* and 6 weeks later, mice were i.p. injected with tamoxifen. 3 days later, a 1 μM cardiotoxin/pinch injury was applied to the gastrocnemius muscle, and HO pathogenesis was assessed at a series of time points post-injury by radiography (heterotopic bone, **e**), at Day 3 by

immunohistochemistry for F4/80 (monocytes/macrophages, **f**) and at Day 7 by Alcian blue staining (fibrosis, chondrogenesis, **f**), Toluidine blue staining (mast cells, **f**), and phospho-SMAD1/5 (BMP signaling, **f**). In (**e**), the red boxes indicate injured areas. RT_2 profiler PCR array (**g**) and RT-PCR analysis (**h**) for inflammatory gene expression were performed on the gastrocnemius muscle 3 days post-injury (day 3). AAV-treated *Acvr1R*$^{(R206H)Fl}$ (control) and *Acvr1R*$^{(R206H)Fl}$;Cre-ER^{T2} muscle RNA with and without *amiR-RH6.ACVR1*^{opt} (gray boxes) are displayed (**h**). Scale bars: 5 mm, **e;** 100 μm, **f**. Values represent mean ± SD: ns, non-significant; *, $P < 0.05$; **, $P < 0.01$; ***, $P < 0.001$; ****, $P < 0.0001$ by one-way ANOVA (**b, c, h**).

Figure 5: Systemic delivery of AAV gene therapy at birth prevents spontaneous HO in juvenile FOP mice

a. 5 x 10^{13} vg/kg of rAAV9.*LacZ* was i.v. injected into 3-week-old *Acvr1*$^{(R206H)Fl}$*;PDGFR*α-cre mice (n=3) and, 2 weeks later, radiography of the whole body was performed to locate HO lesions. Frozen sections of HO tissues were stained for β-galactosidase. Scale bars: 2 mm, **top**; 100 μm, **bottom**. For data shown in **(b-j),** P1 *Acvr1*$^{(R206H)Fl}$ or *Acvr1*$^{(R206H)Fl}$*;PDGFR*α-cre neonates (n=12) were i.v. injected with 10^{11} GCs of rAAV9 carrying *EGFP control, amiR-RH6*, *ACVR1*^{opt}, or *amiR-RH6.ACVR1*^{opt} and AAV-treated mice were analyzed weekly up to 8 weeks of age. **b–c**. Survival curve (**b**) and body weight (**c**) for the AAV-treated groups. **d**. MicroCT analysis for skulls and lumbar vertebrae (L4) of 4 to 5-week-old AAV-treated mice are shown in 3D reconstructed images **(d, top)** and 2D transverse sections **(d, middle and bottom).** Scale bars: 5 mm, **top, middle**; 1 mm, **bottom**. Arrows indicate temporomandibular joint ankylosis. **e–f**. Plots showing the distance of open mouth in 4 to 5-week-old AAV-treated mice **(e)** and the quantification of vertebral bone mass **(f).** AAV-treated *Acvr1R*$^{(R206H)Fl}$ (control) and *Acvr1*$^{(R206H)Fl}$*;PDGFR*α-cre mice (gray boxes) are displayed **(c, e, f)**. Tra. BV/TV: trabecular bone volume per tissue volume. **g**. MicroCT analysis showing the maxillary and mandibular bone mass of AAV-treated mice. 2D cross-section images are displayed. Scale bar: 1 mm. **h.** MicroCT

analysis showing spontaneous HO from whole body scans of AAV-treated mice. 3D reconstructed images **(left)** and 2D transverse sections **(right)** are displayed. Scale bars: 4 mm. **i**. Clinical HO incidence and severity were scored using whole body microCT and radiography**. j.** Safranin O staining of AAV-treated tibias showing normal chondrocyte zones in the growth plate. Scale bars: 50 μm. **k.** P1 *Acvr1*$^{(R206H)Fl}$*;PDGFR*α-cre;*PDGFR*α-GFP reporter neonates were i.v. injected with 10^{11} GCs of rAAV9 carrying mCherry control or *amiR-RH6.ACVR1*^{opt} (n=3) and 5 weeks later, mCherry- and/or GFP-expressing cells in the frozen-sectioned muscle were visualized by fluorescence microscopy. The right panels are enlarged images of the white boxed regions on the left. Scale bars: 100 μm, **left**; 50 μm, **right**. Values represent mean ± SD: ns, non-significant; *, $P < 0.05$; **, $P < 0.01$; ***, $P < 0.001$; ****, $P < 0.0001$ by one-way ANOVA test (**c, e, f, i**).

Figure 6: Systemic delivery of AAV gene therapy at early adulthood prevents spontaneous HO in adult FOP mice

5 x 10^{13} vg/kg of rAAV9 carrying EGFP control or *amiR-RH6.ACVR1*^{opt} was i.v. injected into 6-week-old *Acvr1*$^{(R206H)Fl}$ or *Acvr1*$^{(R206H)Fl}$*;Cre-ER*^{T2} mice (n=10) 3 days after tamoxifen treatment. 12 weeks later, mRNA levels of *ACVR1*^{R206H} and *ACVR1*^{opt} in the liver were assessed by RT-PCR **(a)**. MicroCT analysis showing whole body **(b)**, torso **(c)**, and lower body **(e)** of AAV-treated mice. Arrows indicate HO lesions. Scale bars: 5 mm, **b**; 1 mm, **c, e.** Total HO volume **(d)** and numbers of HO lesions **(f)** throughout the body were quantitated. MicroCT **(g, left)** and histology of knee joints were performed to assess bridging HO **(g, right)**, degeneration of articular cartilage **(h, top)**, and chondrocytes in the growth plate **(h, bottom)**. In **(g)**, the red box, bridging HO; yellow box, articular cartilage and growth plate. Scale bars: 1 mm, **g, left**; 100 μm, **g, right.** Total percentage of clinical HO incidence in AAV-treated mice was assessed **(i)**. Frequency of immune cells within the population of total splenocytes suggests that rAAV9.*amiR-RH6.ACVR1*^{opt} has little to no effect on systemic immunity **(**n=6~8, **j)**. AAV-treated *Acvr1R*$^{(R206H)Fl}$ (control) and *Acvr1*$^{(R206H)Fl}$*;Cre-ER*^{T2} mice (gray boxes) are displayed **(d, f, j)**.

Values represent mean ± SD: ns, non-significant; *, $P < 0.05$; **, $P < 0.01$; ***, $P < 0.001$; and ****, $P < 0.0001$ by an unpaired two-tailed Student's t-test (**a**) or ANOVA test **(d, f, j)**.

Figures

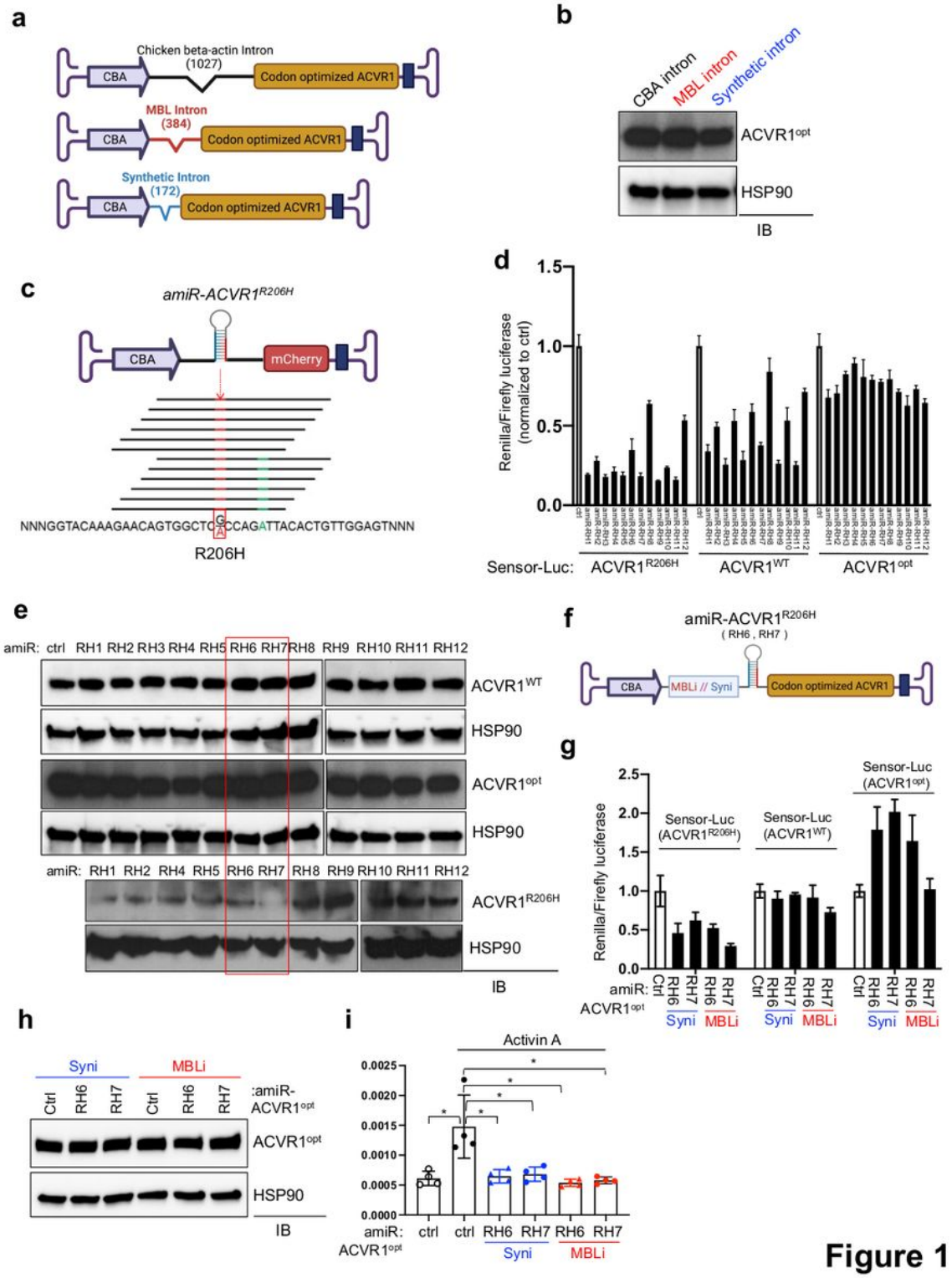

Figure 1

Figure 1

Development of AAV vector targeting the human *ACVR1^{R206H}* receptor

a. Schematic diagram of the plasmids expressing a codon-optimized version of the human ACVR1

complementary DNA (*ACVR1*^{opt}) with the CBA promoter and three different introns. CBA: CMV enhancer/chicken -actin promoter. **b.** Validation of the expression of the ACVR1^{opt} receptor. Plasmids expressing *ACVR1*^{opt} were transiently transfected into HEK293 cells and cell lysates were subjected to immunoblotting with anti-ACVR1 antibody. Anti-HSP90 antibody was used as a loading control. **c.** Schematic diagram representing 12 amiRs that target different sequence sites of human *ACVR1*^{R206H} mRNA (*amiR-ACVR1*^{R206H}). The red box indicates the R206H mutation site (c.617G>A). Adenine (green) was mismatched to increase the selectivity of gene silencing. **d.** Plasmids encoding *amiR-ctrl* or 12 different *amiRs* were transiently transfected into HEK293 cells along with amiR-sensor plasmids (sensor-Luc) that contain *Renilla* luciferase and aimR complimentary sequences for human ACVR1^{R206H}, ACVR1^{WT}, and ACVR1^{opt}. One day later, a luciferase assay was performed to measure *Renilla* luciferase and normalized to firefly luciferase. Lower activities indicate higher silencing efficacy of amiRs. **e.** Plasmids encoding *amiR-ctrl* or 12 different *amiRs* were transiently transfected into HEK293 cells along with a plasmid expressing human ACVR1^{R206H}, ACVR1^{WT}, or ACVR1^{opt} cDNA and immunoblotted for ACVR1. Anti-HSP90 antibody was used for loading control. **f.** Schematic diagram of the combination gene therapy constructs expressing *amiR-ACVR1*^{R206H} (RH6 or RH7) and *ACVR1*^{opt} cDNA under the CBA promoter and MBL intron (MBLi) or synthetic intron (Syni). **g, h.** Plasmids encoding *amiR-ctrl* (ctrl), Syni.amiR-RH6.ACVR1^{opt}, Syni.amiR-RH7.ACVR1^{opt}, MBLi.amiR-RH6.ACVR1^{opt}, or MBLi.amiR-RH7.ACVR1^{opt} were transiently transfected into HEK293 cells along with sensor-Luc plasmids. Luciferase assay **(g)** or immunoblotting analysis for ACVR1 **(h)** was performed. Anti-HSP90 antibody was used for loading control. **i.** Plasmids were transiently transfected into HEK293 cells along with the BMP SMADs-responsive reporter gene (BRE-luc) and treated with Activin A (100 ng/ml). 24 hours later, Activin A signaling activity was measured by luciferase assay. Values represent mean ± SD: *, $P < 0.05$ by an unpaired two-tailed Student's *t*-test or one-way ANOVA test (**i**).

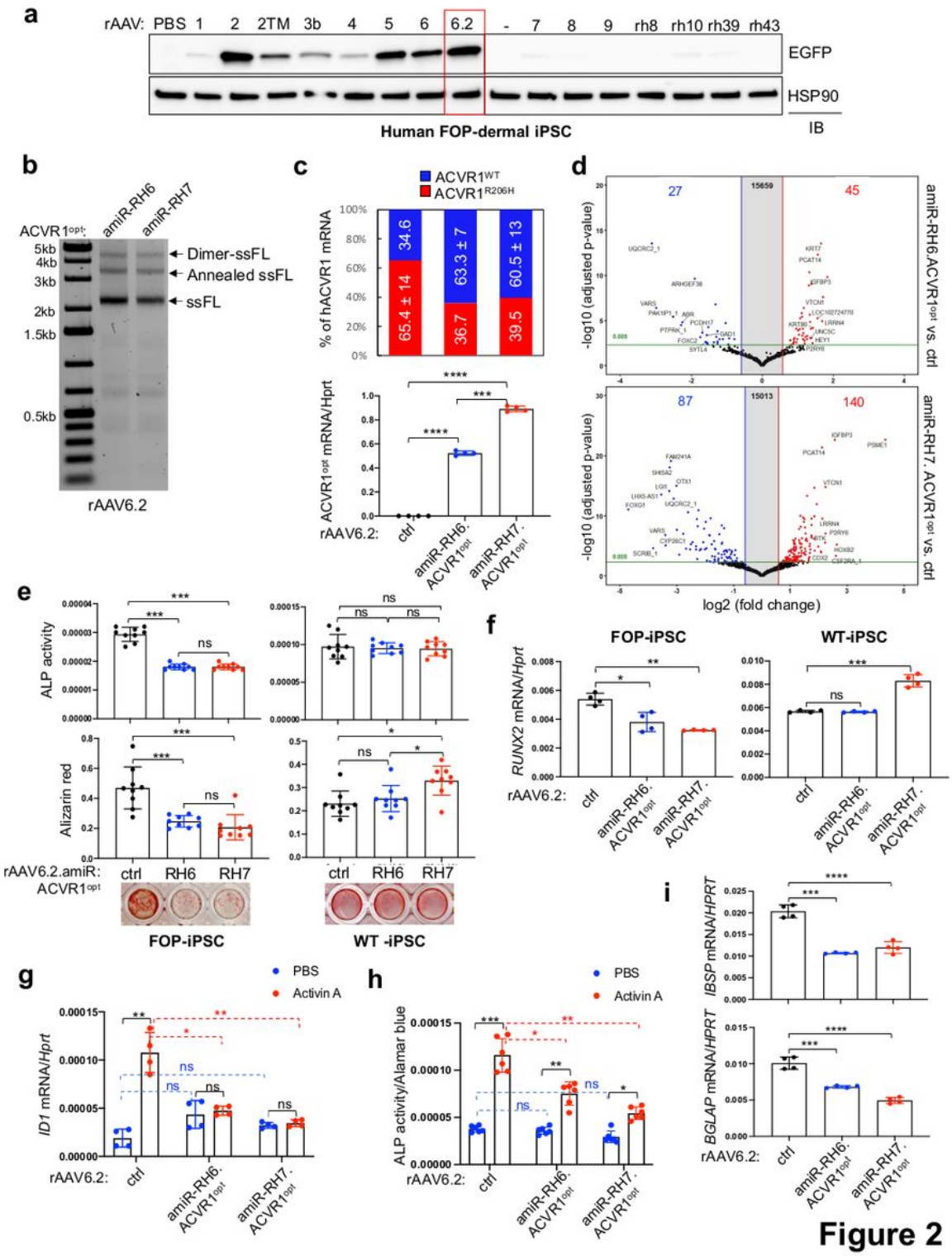

Figure 2

Effects of AAV gene therapy in human FOP iPSCs and mouse *Acvr1*$^{(R206H)KI}$ cells

a. Human FOP iPSCs were treated with PBS or 5 x 10^{10} genome copies (GCs) of 15 different AAV capsids packaged with the same *CBA-Egfp* transgene. 2 days later, EGFP expression was assessed

by immunoblotting with an anti-GFP antibody**.** Anti-HSP90 antibody was used for loading control. **b.** Genome integrity of rAAV6.2 carrying *amiR-RH6.ACVR1^{opt}* or *amiR-RH7.ACVR1^{opt}* was assessed by electrophoresis in native gel. ssFL: single-stranded full-length. **c, d.** 5 x 10^{10} GCs of rAAV6.2 carrying *EGFP control (ctrl), amiR-RH6.ACVR1^{opt}*, or *amiR-RH7.ACVR1^{opt}* were transduced to human FOP iPSCs, cultured under osteogenic conditions for 4 days, and subjected to next-generation sequencing (NGS) for ratio expression: *ACVR1^{R206H} vs. ACVR1^{WT}* (**c, top**) or RT-PCR for *ACVR1^{opt}* expression (**c, bottom**). Alternatively, total RNA was subjected to bulk RNA sequencing (**d**). A volcano plot showing the gene expression for up/downregulated genes in the cells expressing *amiR-RH6.ACVR1^{opt}* or *amiR-RH7.ACVR1^{opt}* relative to *control*-expressing cells is displayed. **e-g.** AAV-treated, human WT or FOP iPSCs were cultured under osteogenic conditions and alkaline phosphatase activity (ALP) and alizarin red staining were performed to assess early and late osteoblast differentiation, respectively (**e**). Alternatively, osteogenic gene expression (Runx2) was assessed by RT-PCR (**f**). AAV-treated, human FOP iPSCs were incubated with PBS or Activin A (100 ng/ml) for 6 hours, and *ID1* mRNA levels were measured by RT-PCR (**g**). **h, i.** PDGFR $^{+}$Sca1^{+}CD31^{-}CD45^{-} FAPs were sorted by FACS from the digested skeletal muscle of 4-week-old *Acvr1$^{(R206H)Fl}$;PDGFR*-cre mice and transduced with 5 x 10^{10} GCs of AAV6.2 carrying *EGFP control, amiR-RH6.ACVR1^{opt}*, or *amiR-RH7.ACVR1^{opt}*. 2 days later, AAV-treated FAPs were cultured under osteogenic conditions with PBS or Activin A (50 ng/ml) for 6 days, and ALP activity (**h**) and osteogenic gene expression (BGLAP, IBSP, **i**) were assessed for osteoblast differentiation. Values represent mean ± SD: ns, non-significant; *, P <0.05; **, P < 0.01; ***, P < 0.001; ****, P < 0.0001 by an unpaired two-tailed Student's t-test or one-way ANOVA test (**e-i**).

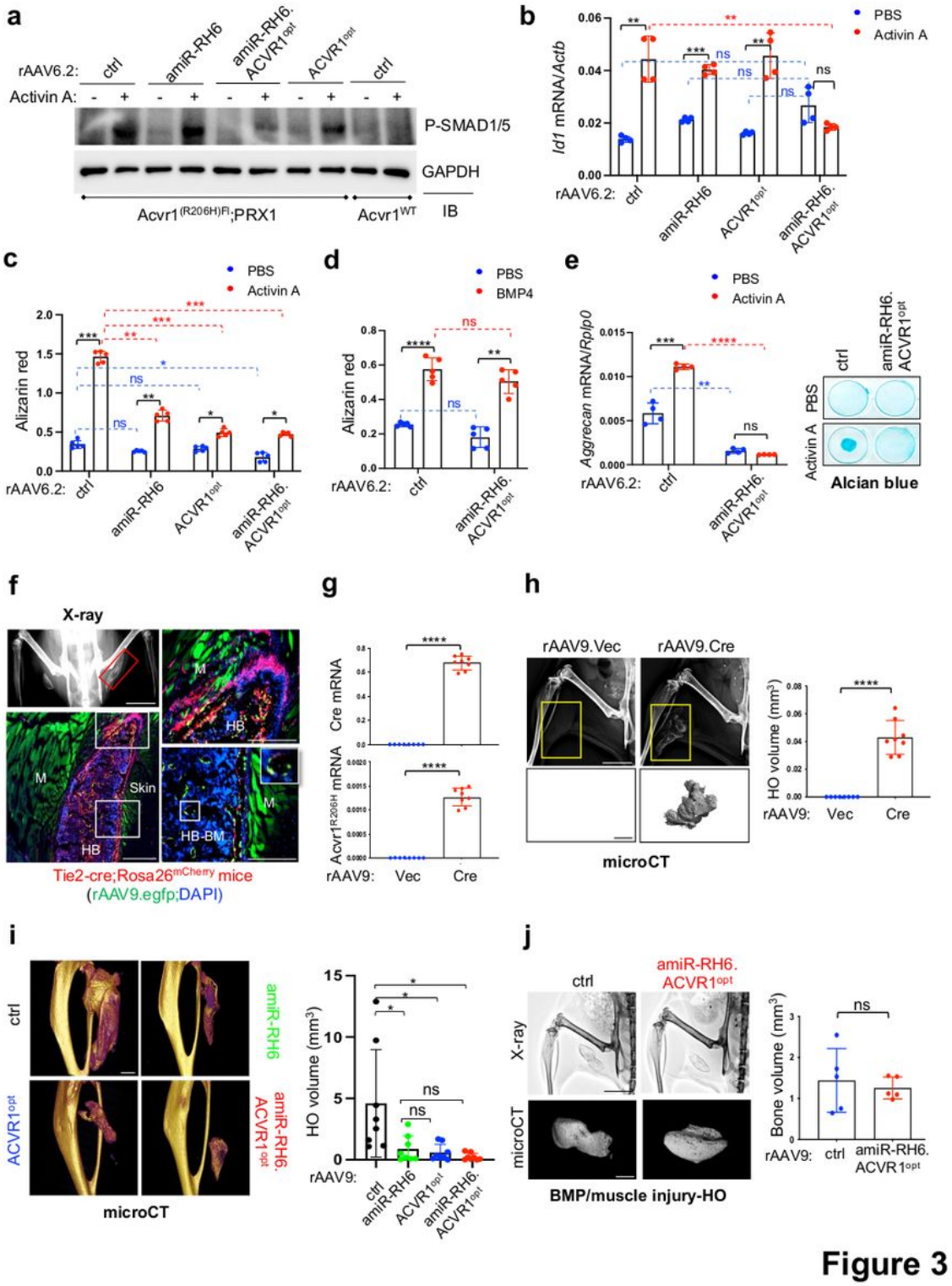

Figure 3

Figure 3

AAV gene therapy suppresses Activin A signaling and trauma-induced HO a–d. *PRRX1*$^{+}$ osteogenic progenitors were isolated from the long bones of 4-week-old *PRRX1-cre*

(*Acvr1*^{WT}) or *Acvr1*$^{(R206H)Fl}$*;PRRX1-cre* mice and transduced with 5 x 10^{10} GCs of AAV6.2 carrying *EGFP*

control, amiR-RH6, ACVR1^{opt}, or *amiR-RH6.ACVR1^{opt}*. 2 days later, AAV-treated cells were stimulated with Activin A (100 ng/ml) for 30 min and immunoblotted for phospho-SMAD1/5. Anti-GAPDH antibody was used for loading control (**a**). 6 hours after Activin A stimulation*, Id1* mRNA levels were assessed by RT-PCR (**b**). AAV-treated cells were cultured under osteogenic conditions with PBS, Activin A (50 ng/ml, **c**), or BMP4 (50 ng/ml, **d**) for 12 days, and Alizarin red staining was performed to detect mineralization. **e.** *PRRX1^{+}* chondrogenic progenitors were isolated from the knee joints of P2 *Acvr1$^{(R206H)Fl}$;PRRX1-cre* neonates, transduced with AAV6.2 carrying *EGFP control* or *amiR-RH6.ACVR1^{opt}*, and cultured under chondrogenic conditions for 4 or 6 days. *Aggrecan* mRNA levels or Alcian blue staining were performed for chondrogenesis assessment. **f.** 5 x 10^{12} vg/kg of rAAV9.*egfp* was t.d. injected into the quadricep of 2-month-old *Tie2-cre;Rosa26^{mCherry}* mice that label Tie^{+} FAPs and endothelial cells (red, n=3) using a hollow microneedle 1 week after i.m. injection with rBMP2/7/matrigel and muscle injury. 3 weeks later, radiography of hindlimbs and histology on frozen sections of HO tissues were performed to visualize GFP-expressing FAP-lineage cells. The red box indicates a heterotopic bone (HB) in the skeletal muscle. DAPI was used for nuclear staining. M, muscle; HB-BM, heterotopic bone-bone marrow. Scale bars: 5 mm, **left top**; 500 μm, **left bottom**; 400 μm, **right. g, h.** 5 x 10^{12} vg/kg of rAAV9 expressing vector control (Vec) or Cre recombinase was t.d. injected into the hindlimb of 6-week-old *Acvr1R$^{(R206H)Fl}$* mice (n=8), and 1 mM cardiotoxin/pinch injury was introduced into

the gastrocnemius muscle 3 days post-injection. 4 weeks later, mRNA levels of *ACVR1^{R206H}* and *Cre* recombinase were assessed by RT-PCR **(g)** and heterotopic bone volume was detected by radiography and quantified by microCT **(h).** 3D reconstruction images and quantification of HO volume are displayed. Scale bars: 5 mm, **left top**; 1 mm, **left bottom**. **i.** For trauma-induced HO in FOP mice, 5 x 10^{12} vg/kg of rAAV9 carrying *EGFP control, amiR-RH6, ACVR1^{opt}*, or *amiR-RH6.ACVR1^{opt}* was t.d. injected into the hindlimbs of 6-week-old *Acvr1R$^{(R206H)Fl}$;Cre-ER^{T2}* mice (n=8) 3 days post-injection of

tamoxifen (10 mg/kg). A 1 mM cardiotoxin/pinch injury was applied to the gastrocnemius muscle 3 days post-injection. 4 weeks later, HO was assessed by microCT. 3D reconstruction images and quantification of HO volume are displayed. Scale bar: 1 mm. **j.** For trauma-induced HO in WT mice, 5 x 10^{12} vg/kg of rAAV9 expressing *EGFP control* or *amiR-RH6.ACVR1^{opt}* was t.d. injected into the quadricep of 2-month-old WT mice (n=5) followed by an rBMP2/7/matrigel injection and a muscle injury. 4 weeks later, HO was assessed by radiography and microCT. 3D reconstruction images and quantification of HO volume are displayed**.** Scale bars: 5 mm, **top**; 1 mm, **bottom.** Values represent mean ± SD: ns, non-significant; *, $P < 0.05$; **, $P < 0.01$; ***, $P < 0.001$; and ****, $P < 0.0001$ by an unpaired two-tailed Student's t-test or one-way ANOVA test (**b-e, g-j**).

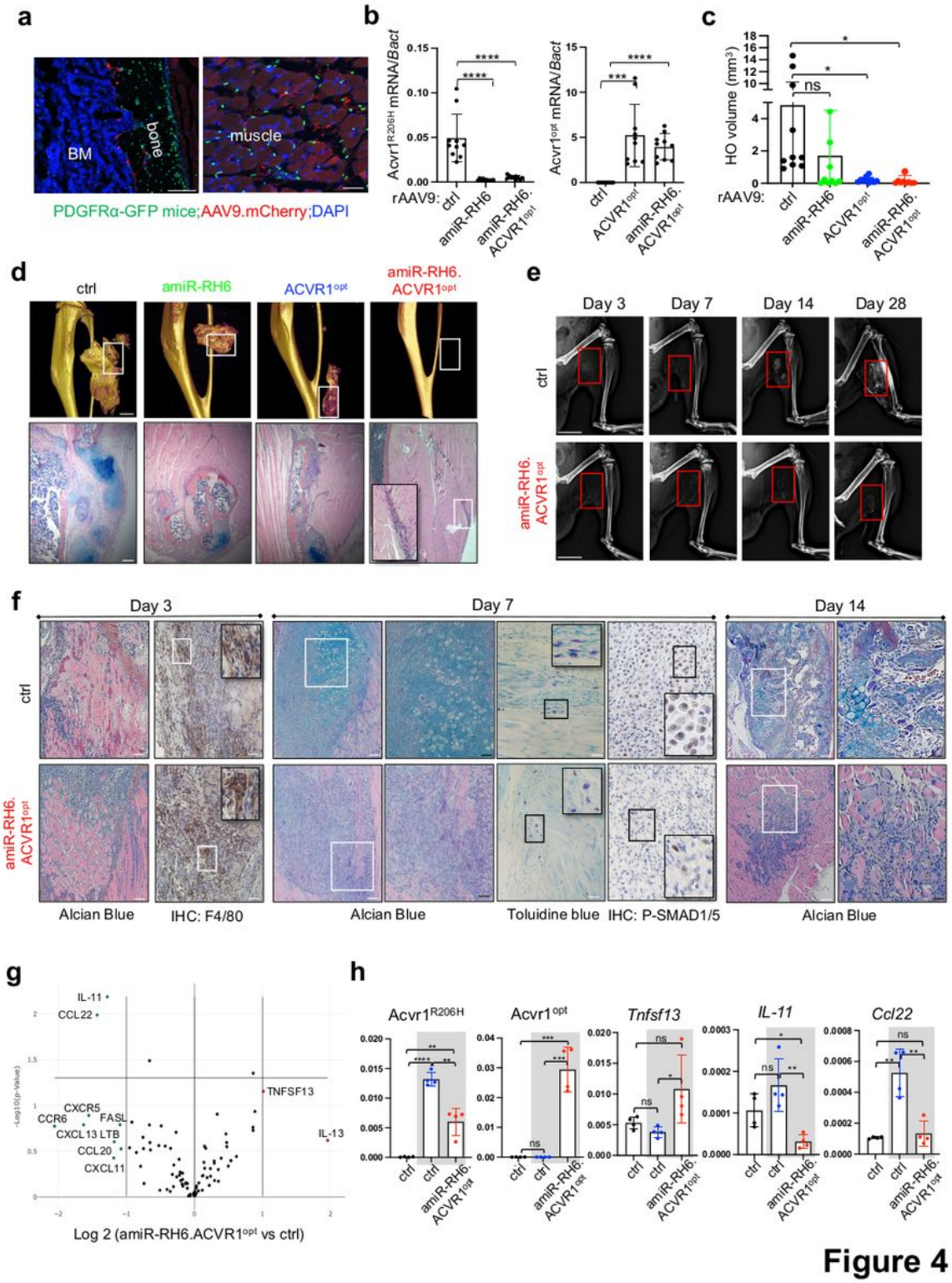

Figure 4

Figure 4

Systemic delivery of AAV gene therapy at birth prevents traumatic HO in FOP mice

a. P1 PDGFR -GFP reporter neonates (n=3) were i.v. injected with 10^{11} GCs of rAAV9 expressing mCherry and 2 weeks later, mCherry and GFP expression in frozen sections of AAV-treated tibia and

muscle was assessed by fluorescence microscopy. BM: bone marrow. Scale bars: 100 μm, **left**; 50 μm, **right**. **b-d.** P1 *Acvr1*$^{(R206H)Fl}$*;Cre-ER*^{T2} neonates (n=10) were i.v. injected with 10^{11} GCs of rAAV9 carrying *EGFP control, amiR-RH6, ACVR1*^{opt}, or *amiR-RH6.ACVR1*^{opt} and 6 weeks later, mice were treated with tamoxifen (10 mg/kg). A 1 mM cardiotoxin/pinch injury was applied to the gastrocnemius muscle 3 days post-tamoxifen treatment. 4 weeks later, mRNA levels of *ACVR1*^{R206H} and *ACVR1*^{opt} were measured by RT-PCR **(b)** and HO in the gastrocnemius muscle was assessed by microCT and histology **(c, d)**. 3D reconstruction images **(d)** and quantification of HO volume **(c)** are displayed**.** Alcian blue staining of HO tissues **(d)** was performed to assess chondrogenic anlagen. Scale bars: 1 mm, **top**; 200 μm, **bottom**. **e-h.** To investigate the progression of HO pathogenesis, P1 *Acvr1R*$^{(R206H)Fl}$ or *Acvr1R*$^{(R206H)Fl}$*;Cre-ER*^{T2} neonates (n=3) were i.v. injected with 10^{11} GCs of rAAV9 carrying *EGFP control* or *amiR-RH6.ACVR1*^{opt} and 6 weeks later, mice were i.p. injected with tamoxifen. 3 days later, a 1 mM cardiotoxin/pinch injury was applied to the gastrocnemius muscle, and HO pathogenesis was assessed at a series of time points post-injury by radiography (heterotopic bone, **e**), at Day 3 by immunohistochemistry for F4/80 (monocytes/macrophages, **f**) and at Day 7 by Alcian blue staining (fibrosis, chondrogenesis, **f**), Toluidine blue staining (mast cells, **f**), and phospho-SMAD1/5 (BMP signaling, **f**). In (**e**), the red boxes indicate injured areas. RT2 profiler PCR array (**g**) and RT-PCR analysis (**h**) for inflammatory gene expression were performed on the gastrocnemius muscle 3 days post-injury (day 3). AAV-treated *Acvr1R*$^{(R206H)Fl}$ (control) and *Acvr1R*$^{(R206H)Fl}$;Cre-ER^{T2} muscle RNA with and without *amiR-RH6.ACVR1*^{opt} (gray boxes) are displayed (**h**). Scale bars: 5 mm, **e;** 100 μm, **f**. Values represent mean ± SD: ns, non-significant; *, $P < 0.05$; **, $P < 0.01$; ***, $P < 0.001$; ****, $P < 0.0001$ by one-way ANOVA (**b, c, h**).

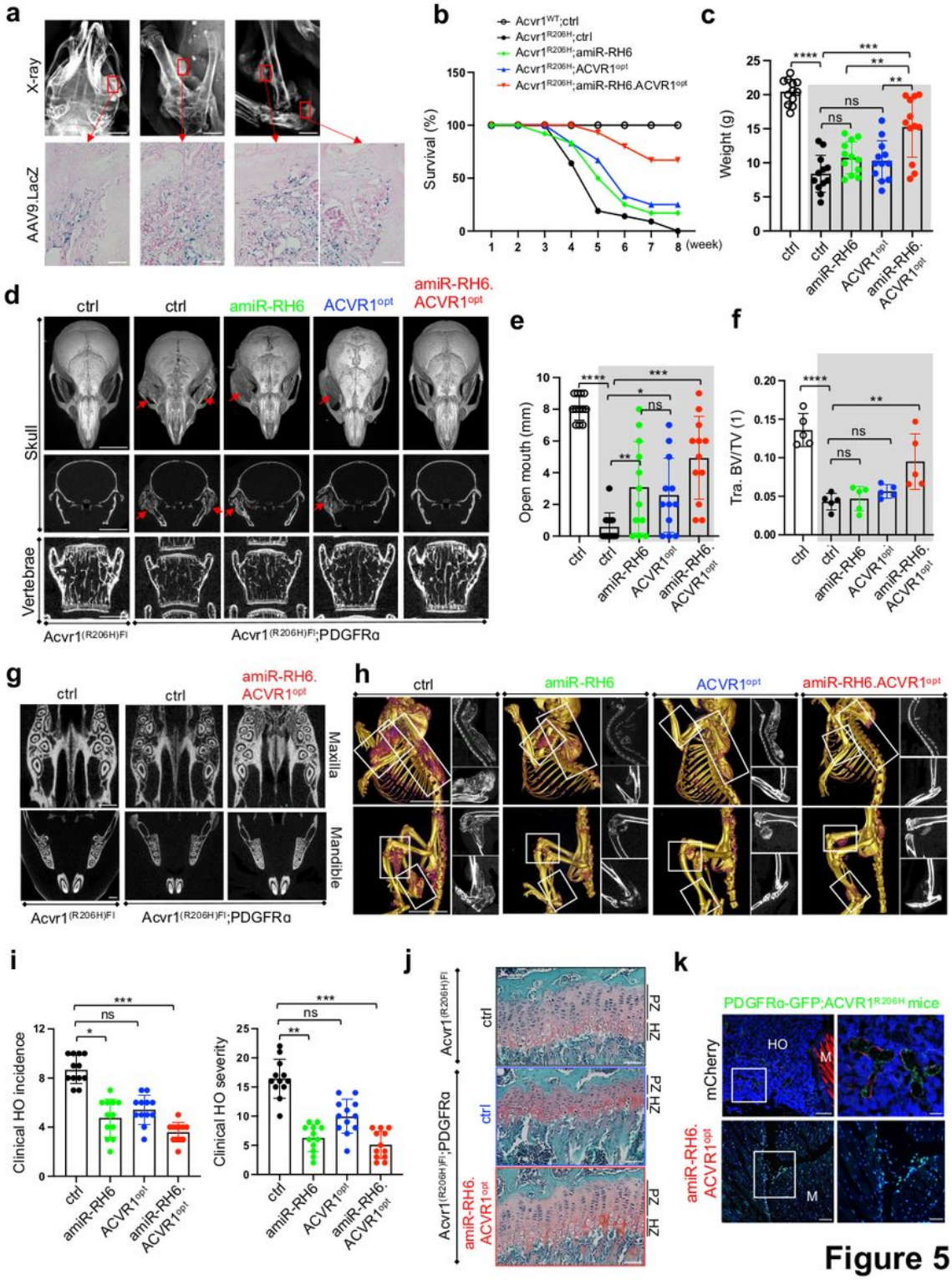

Figure 5

Figure 5

Systemic delivery of AAV gene therapy at birth prevents spontaneous HO in juvenile FOP mice

a. 5 x 10^{13} vg/kg of rAAV9.*LacZ* was i.v. injected into 3-week-old *Acvr1*$^{(R206H)Fl}$*;PDGFR*-cre mice (n=3)

and, 2 weeks later, radiography of the whole body was performed to locate HO lesions. Frozen sections of HO tissues were stained for -galactosidase. Scale bars: 2 mm, **top**; 100 μm, **bottom**. For data shown in **(b-j),** P1 *Acvr1*$^{(R206H)Fl}$ or *Acvr1*$^{(R206H)Fl}$*;PDGFR* -cre neonates (n=12) were i.v. injected with 10^{11} GCs of rAAV9 carrying *EGFP control, amiR-RH6*, *ACVR1*^{opt}, or *amiR-RH6.ACVR1*^{opt} and AAV-treated mice were analyzed weekly up to 8 weeks of age. **b–c**. Survival curve (**b**) and body weight (**c**) for the AAV-treated groups. **d**. MicroCT analysis for skulls and lumbar vertebrae (L4) of 4 to 5-week-old AAV-treated mice are shown in 3D reconstructed images **(d, top)** and 2D transverse sections **(d, middle and bottom).** Scale bars: 5 mm, **top, middle**; 1 mm, **bottom**. Arrows indicate temporomandibular joint ankylosis. **e–f**. Plots showing the distance of open mouth in 4 to 5-week-old AAV-treated mice **(e)** and the quantification of vertebral bone mass **(f).** AAV-treated *Acvr1R*$^{(R206H)Fl}$ (control) and *Acvr1*$^{(R206H)Fl}$*;PDGFR* -cre mice (gray boxes) are displayed **(c, e, f)**. Tra. BV/TV: trabecular bone volume per tissue volume. **g**. MicroCT analysis showing the maxillary and mandibular bone mass of AAV-treated mice. 2D cross-section images are displayed. Scale bar: 1 mm. **h.** MicroCT analysis showing spontaneous HO from whole body scans of AAV-treated mice. 3D reconstructed images **(left)** and 2D transverse sections **(right)** are displayed. Scale bars: 4 mm. **i**. Clinical HO incidence and severity were scored using whole body microCT and radiography**. j.** Safranin O staining of AAV-treated tibias showing normal chondrocyte zones in the growth plate. Scale bars: 50 μm. **k.** P1 *Acvr1*$^{(R206H)Fl}$*;PDGFR* -cre;*PDGFR* -GFP reporter neonates were i.v. injected with 10^{11} GCs of rAAV9 carrying mCherry control or *amiR-RH6.ACVR1*^{opt} (n=3) and 5 weeks later, mCherry- and/or GFP-expressing cells in the frozen-sectioned muscle were visualized by fluorescence microscopy. The right panels are enlarged images of the white boxed regions on the left. Scale bars: 100 μm, **left**; 50 μm, **right**. Values represent mean ± SD: ns, non-significant; *, $P < 0.05$; **, $P < 0.01$; ***, $P < 0.001$; ****, $P < 0.0001$ by one-way ANOVA test (**c, e, f, i**).

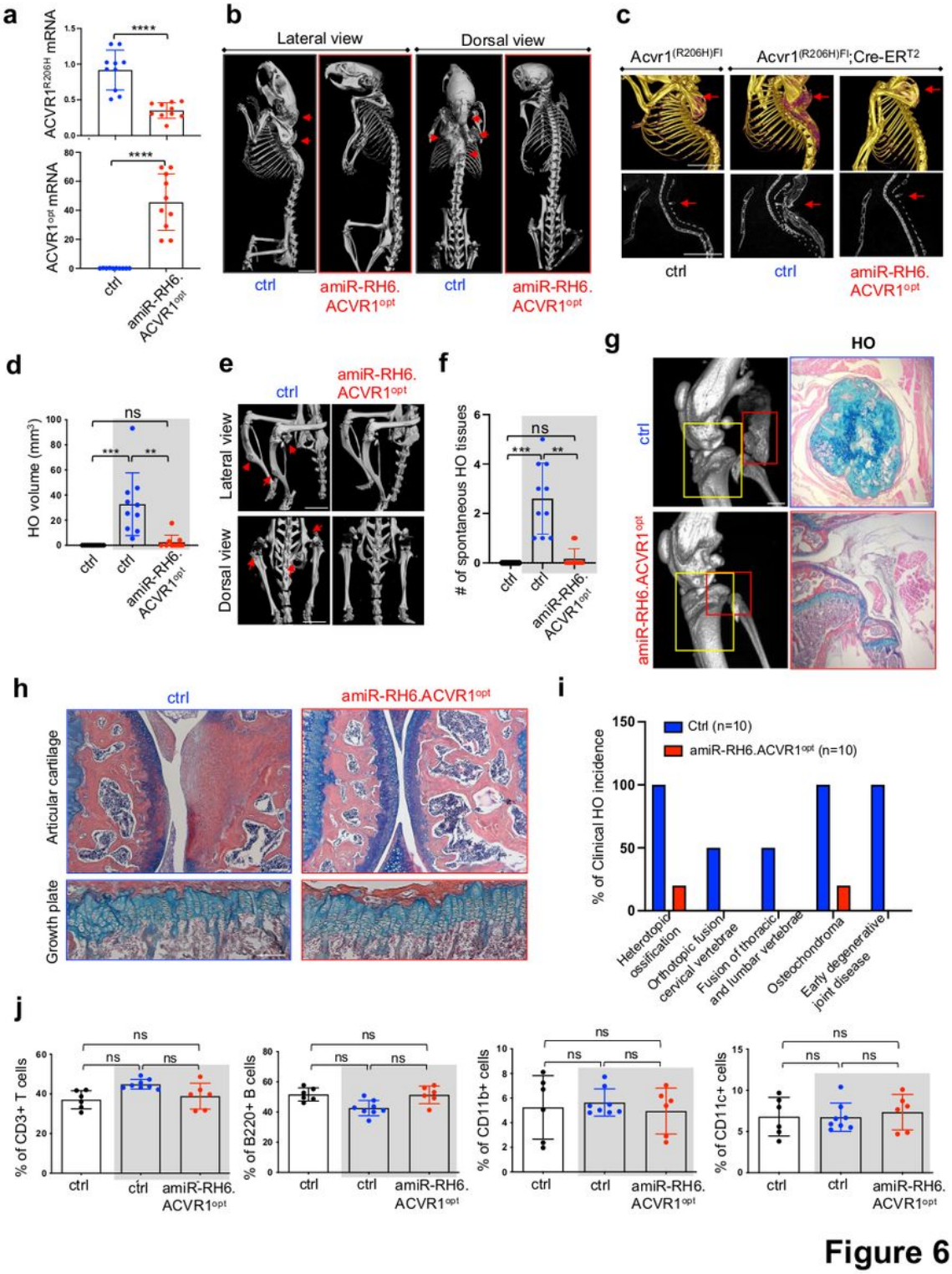

Figure 6

Figure 6

Systemic delivery of AAV gene therapy at early adulthood prevents spontaneous HO in adult FOP mice

5 x 10^{13} vg/kg of rAAV9 carrying EGFP control or *amiR-RH6.ACVR1^{opt}* was i.v. injected into 6-week-old

Acvr1$^{(R206H)Fl}$ or *Acvr1*$^{(R206H)Fl}$*;Cre-ER*^{T2} mice (n=10) 3 days after tamoxifen treatment. 12 weeks later, mRNA levels of *ACVR1*^{R206H} and *ACVR1*^{opt} in the liver were assessed by RT-PCR **(a)**. MicroCT analysis showing whole body **(b)**, torso **(c)**, and lower body **(e)** of AAV-treated mice. Arrows indicate HO lesions. Scale bars: 5 mm, **b**; 1 mm, **c, e.** Total HO volume **(d)** and numbers of HO lesions **(f)** throughout the body were quantitated. MicroCT **(g, left)** and histology of knee joints were performed to assess bridging HO **(g, right)**, degeneration of articular cartilage **(h, top)**, and chondrocytes in the growth plate **(h, bottom)**. In **(g)**, the red box, bridging HO; yellow box, articular cartilage and growth plate. Scale bars: 1 mm, **g, left**; 100 μm, **g, right.** Total percentage of clinical HO incidence in AAV-treated mice was assessed **(i)**. Frequency of immune cells within the population of total splenocytes suggests that rAAV9.*amiR-RH6.ACVR1*^{opt} has little to no effect on systemic immunity **(**n=6~8, **j)**. AAV-treated *Acvr1R*$^{(R206H)Fl}$ (control) and *Acvr1*$^{(R206H)Fl}$*;Cre-ER*^{T2} mice (gray boxes) are displayed **(d, f, j)**. Values represent mean ± SD: ns, non-significant; *, $P < 0.05$; **, $P < 0.01$; ***, $P < 0.001$; and ****, $P < 0.0001$ by an unpaired two-tailed Student's t-test (**a**) or ANOVA test **(d, f, j)**.

Supplementary Files

This is a list of supplementary files associated with this preprint. Click to download.

- movie3.mp4
- SuppfiguresNC.pdf
- movie2.mp4
- YenetalSuppTextNC.pdf
- Movie1.mov
- movie4.mov